AD-A060 612 ARMY ARMAMENT RESEARCH AND DEVELOPMENT COMMAND ABERD--ETC F/G 4/1
SOURCE: A FORTRAN-IV SUBROUTINE PACKAGE THAT MODELS SEVERAL NAT--ETC(U)
AUG 78 I L CHIDSEY

UNCLASSIFIED ARBRL-TR-02093 SBIE-AD-E430 108 NL

1 OF 1
AD A060612

END
DATE FILMED
1-79
DDC

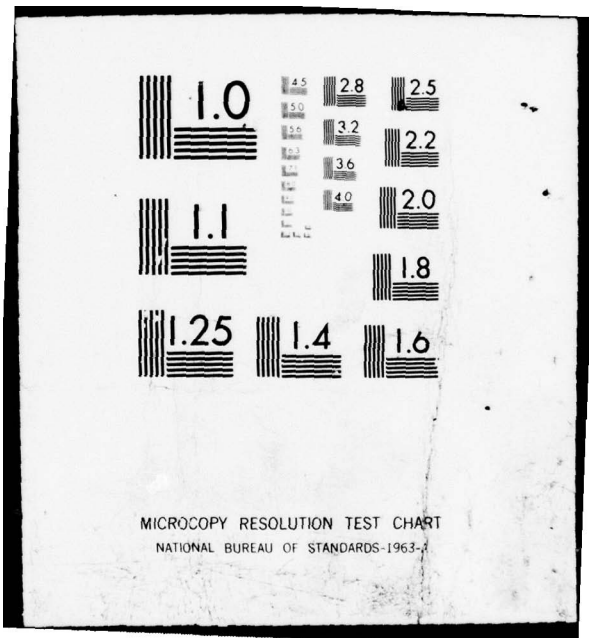
1.0
1.1
1.25
1.4
1.6
1.8
2.0
2.2
2.5
2.8
3.2
3.6
4.0
4.5
5.0
5.6
MICROCOPY RESOLUTION TEST CHART
NATIONAL BUREAU OF STANDARDS-1963-A

12 LEVEL I

19 AD-E430 198

18 SBIE

9 TECHNICAL REPORT 14 ARBRL-TR-02093

6 SOURCE: A FORTRAN-IV SUBROUTINE PACKAGE THAT MODELS SEVERAL NATURALLY OCCURRING ENERGY INPUTS TO THE MESOSPHERE.

10 Irving L. Chidsey

12 51 p.

11 August 1978



US ARMY ARMAMENT RESEARCH AND DEVELOPMENT COMMAND
BALLISTIC RESEARCH LABORATORY
ABERDEEN PROVING GROUND, MARYLAND

16 1L161102B53A

Approved for public release; distribution unlimited.

393 471

78 09 11 022

Destroy this report when it is no longer needed.
Do not return it to the originator.

Secondary distribution of this report by originating or sponsoring activity is prohibited.

Additional copies of this report may be obtained from the National Technical Information Service, U.S. Department of Commerce, Springfield, Virginia 22161.

The findings in this report are not to be construed as an official Department of the Army position, unless so designated by other authorized documents.

*The use of trade names or manufacturers' names in this report does not constitute indorsement of any commercial product.*

UNCLASSIFIED

SECURITY CLASSIFICATION OF THIS PAGE (When Data Entered)

## REPORT DOCUMENTATION PAGE

READ INSTRUCTIONS BEFORE COMPLETING FORM

1. REPORT NUMBER: TECHNICAL REPORT ARBRL-TR-02093
2. GOVT ACCESSION NO.
3. RECIPIENT'S CATALOG NUMBER

4. TITLE (and Subtitle): SOURCE: A FORTRAN-IV SUBROUTINE PACKAGE THAT MODELS SEVERAL NATURALLY OCCURRING ENERGY INPUTS TO THE MESOSPHERE
5. TYPE OF REPORT & PERIOD COVERED
6. PERFORMING ORG. REPORT NUMBER

7. AUTHOR(s): Irving L. Chidsey
8. CONTRACT OR GRANT NUMBER(s)

9. PERFORMING ORGANIZATION NAME AND ADDRESS
US Army Ballistic Research Laboratory
ATTN: DRDAR-BLB
Aberdeen Proving Ground, MD 21005
10. PROGRAM ELEMENT, PROJECT, TASK AREA & WORK UNIT NUMBERS
RDT&E 1L116102B53A

11. CONTROLLING OFFICE NAME AND ADDRESS
US Army Armament Research & Development Command
US Army Ballistic Research Laboratory
ATTN: DRDAR-BL
Aberdeen Proving Ground, MD 21005
12. REPORT DATE: AUGUST 1978
13. NUMBER OF PAGES: 53

14. MONITORING AGENCY NAME & ADDRESS (if different from Controlling Office)
15. SECURITY CLASS. (of this report): Unclassified
15a. DECLASSIFICATION/DOWNGRADING SCHEDULE

16. DISTRIBUTION STATEMENT (of this Report)

Approved for public release; distribution unlimited.

17. DISTRIBUTION STATEMENT (of the abstract entered in Block 20, if different from Report)



18. SUPPLEMENTARY NOTES

19. KEY WORDS (Continue on reverse side if necessary and identify by block number)

| | |
|---|---|
| Ionospheric Modelling | Precipitating Electrons |
| D-Region Modelling | Solar Photons |
| Mesosphere | Eclipse Effects |
| Cosmic Rays | Photolytic Reactions |

20. ABSTRACT (Continue on reverse side if necessary and identify by block number) (eal)

This report documents the natural energy input models used in the BENCHMARK-76 and ECLIPSE-66 studies. Energy sources included are solar x-rays, solar ultraviolet and visible light, galactic cosmic rays, and precipitated electrons. These energy sources and their interactions with the atmosphere were modeled over the range 40-100 km altitude.

DD FORM 1 JAN 73 1473 EDITION OF 1 NOV 65 IS OBSOLETE

UNCLASSIFIED

SECURITY CLASSIFICATION OF THIS PAGE (When Data Entered)

TABLE OF CONTENTS

## LIST OF TABLES

## INTRODUCTION

The interaction between the chemical species which make up the upper atmosphere and the energy sources which drive the atmospheric chemistry are primarily two-body 2nd order reactions between the resident chemical species and the flux of incoming photons and energetic particles. The rate constants for the reactions are expressed as interaction cross-sections which can and often do vary rapidly with available energy in addition to being different for each chemical species. Treating these reactions in a straightforward way as two-body reactions and adding them to any atmospheric reaction set would result in an essentially uncalculatable set. The deliberately broad band source models described in this report, which model energy inputs with only 47 solar bands plus photoelectrons, precipitated electrons, and galactic cosmic rays, would be prohibitively unwieldy if combined with the 45 basic chemical species-photon interaction reactions in the ECLIPSE-66 set,[1] or the 60 basic reactions in the BENCHMARK-76 set.[2] After allowing for those rate constants which are zero in the present sets, or would be zero in the full set, we get an increase from perhaps 40 basic reactions to about 2000 for these two cases.

It is therefore customary to reduce these photon-species reactions to psuedo-first order reactions by taking the sum

$$k_n = \sum_i \phi_i \sigma_{in}$$

where

$n \equiv$ the number of the pseudo first order reaction

$i \equiv$ the wavelength band number

$k \equiv$ psuedo-first order rate constant

$\phi \equiv$ photon flux

$\sigma \equiv$ interaction cross section.

---

[1] F. E. Niles and I. L. Chidsey, "Comparison of Measured and Calculated D-Region Electron Density for Solar Eclipse of 12 November 1966," and I. L. Chidsey and F. E. Niles, "Comparison of Measured and Calculated D-Region Positive-Ion Number Density for Solar Eclipse of 12 November 1966," Trans. AGU 56, 997 (1975).

[2] J. M. Heimerl and F. E. Niles, "BENCHMARK-76 Model Computations for Disturbed Atmospheric Conditions, I. Input Parameters," BRL Report No. 2022, October 1977; "BENCHMARK-76 Model Computations for Disturbed Atmospheric Conditions, II. Results for the Stratosphere and Mesosphere," BRL Report ARBRL-TR-02050, March 1978; and "BENCHMARK-76 Model Computations for Disturbed Atmospheric Conditions, III. Results for Selected Excitation Parameters at 60 km," BRL Report ARBRL-TR-02051, April 1978. (AD Nos. A050355, A054325, and A054376)

This report documents how we obtained these psuedo-first order rate constants for two studies, ECLIPSE-66[1] and BENCHMARK-76.[2]

For the ECLIPSE-66 study the time variation of these reaction rate constants was critical, and they were computed by a subroutine package which was a part of the ECLIPSE-66 computer program.

For the BENCHMARK-76 study the time variations were not of interest and the subroutine package was used as a separate program. The output of this "stand-alone" program was a table of psuedo-first order rate constants as a function of altitude and is recorded as Table 9 of the Appendix. [See also Table 3 of reference 2 (I).]

## ENERGY SOURCES

The code contains models of several sources of energy: the sun, including x-rays, and ultraviolet and visible light; precipitated electrons; and galactic cosmic rays. The solar model requires a separate atmospheric attenuation model; the precipitating electron model includes atmospheric attenuation; the cosmic ray model ignores it. The eclipse study also required an eclipse model.

## NON-IONIZING SOURCES

The only source of non-ionizing energy in the code is the sun. Although the visible light and most of the ultraviolet light are unable to produce the ionization we are trying to study, the enormous amounts of non-ionizing radiation relative to the ionizing radiation drive most of the neutral chemistry and can strongly modulate the charged particle chemistry.

The Solar Model, which is given in Table 1 of the Appendix is based on that used in the OPTIR II code.[3] The OPTIR II Solar Model covers the ultraviolet from 100 to 400 nm in 30 bands each 0.25 $\mu m^{-1}$ wide. (The inverse micrometer ($\mu m^{-1}$) is a measure of wave number or energy similar to the inverse centimeter.) We chose to base our solar model on the OPTIR II model because it is made up of a few wide bands rather than many narrow bands and is given in units of photon flux rather than of energy flux. This model was extended on the short wavelength side by ten x-ray bands: three bands 0.2 nm wide from 0.4 to 1.0 nm, and seven bands nominally 1.0 nm wide from 3.1 to 10.0 nm. The x-ray photon fluxes for bands 1-3 were taken from Figure 3 of Sears review of November

---

[3] O. P. Manley, H. J. P. Smith, Y. M. Treve, J. W. Carpenter, T. C. Degges, and L. R. Doone, "OPTIR II," AFCRL-71-0528 (1), AFCRL, Bedford, MA, 1971.

1966 eclipse[4] measurements with the conversion from ergs $cm^{-2}$ $sec^{-1}$ to photons $cm^{-2}$ $sec^{-1}$ computed for the center of each band. Because Sears' energy fluxes for bands 4-10 are approximately 5 times those recommended by Swider[5] for 'quiet' solar conditions we used 5 times Swider's 'quiet' model for our model. Again, we converted from ergs $cm^{-2}$ $sec^{-1}$ to photons $cm^{-2}$ $sec^{-1}$ at the band center.

The long wavelength limit of the OPTIR solar model was extended from 400 nm to 735 nm by adding seven bands, the width of each being about 10% of center wavelength. These were obtained by combining bands from Ackerman's[6] model, as shown in Table 1.

Our 47 band model requires about 2200 words of memory when used with our 5 absorbing species and 60 photolytic reactions. Direct use of Ackerman's model would have quadrupled both memory requirements and the number of photon interaction calculations such as absorption, dissociation, etc.

## IONIZING RADIATIONS

For computational purposes it was convenient to consider four sources of ionization: solar ultraviolet, solar x-rays, galactic cosmic rays, and precipitating electrons. The solar ultraviolet ionization source comprises bands 11-20 of the solar model mentioned above. The solar x-ray source comprises bands 1-10 of the solar model and includes ionization by two processes: primary photo-ionization and secondary ionization due to energetic photo-electrons.

The Photoelectron Pair Production Model supplements the x-ray portion of the solar model. The x-ray photons have considerable energy beyond that required to ionize atmospheric chemical species, and this energy appears as kinetic energy of the photoelectrons plus a small contribution from multiply-charged ions.[5] These photoelectrons plus any multiply-charged ions create secondary ionization in the vicinity of the primary photon absorption.[3] This secondary ion-pair production is given by

---

[4] R. D. Sears, "Analysis of the 1966 Solar Eclipse Data," LMSC D246526, Lockheed Palo Alto Research Lab, Palo Alto, CA, 1972.

[5] W. Swider, Jr., "Ionization Rates Due to the Attenuation of 1-100Å Nonflare Solar X-Rays," Rev. Geophys. 7, No. 3, 573-594 (August 1969).

[6] M. Ackerman, "Ultraviolet Solar Radiation Related to Mesospheric Processes," in Mesospheric Models and Related Experiments, G. Fiacco, ed., Springer Verlag, N.Y., 149-159 (1971).

TABLE 1. DERIVATION OF BRL BANDS 41 - 47 FROM ACKERMAN'S SOLAR MODEL[6]

| Ackerman's Bands | BRL Band | Photons $10^{16}(cm^{-2}sec^{-1})$ | Wavelength Range (nm) |
|---|---|---|---|
| 113-118 | 41 | 1.145 | 400-435 |
| 119-126 | 42 | 1.851 | 435-470 |
| 127-134 | 43 | 2.015 | 470-510 |
| 135-144 | 44 | 2.581 | 510-560 |
| 145-156 | 45 | 3.237 | 560-620 |
| 157-165 | 46 | 3.040 | 620-680 |
| 166-171 | 47 | 3.528 | 680-735 |

$$Pairs_{Phe} = 0.03 \left(\sum_i E_i \sigma_i I_i\right) - 1$$

where

$Pairs_{Phe}$ ≡ photo-electron pair production

$E_i$ ≡ energy per photon in electron volts

$\sigma_i$ ≡ ionization cross section in $10^{-22}$ $M^2$

$I_i$ ≡ the attenuated photon flux in photons $cm^{-2}$ $sec^{-1}$

0.03 ≡ the approximate ionization efficiency in ion-pairs per electron volt.

i ≡ the solar x-ray band number.

The one in this expression accounts for the initial ionization reaction.

The Galactic Cosmic Ray ionization constant used was $3.6 \times 10^{-18}$ $molecules^{-1}$ $cm^{-3}$ $sec^{-1}$ and was obtained by linear interpolation between Sears' equations 1 and 2

$$Q_{GCR\ max} = 4(30 + 250 \sin^4\lambda) \times 10^{-20}\ n$$

$$Q_{GCR\ min} = 4(30 + 1000 \sin^4\lambda) \times 10^{-20}\ n$$

where $\lambda$ ≡ the geomagnetic latitude

$n$ ≡ number density per $cm^3$

for a geomagnetic latitude of 32.4°S[4] and is consistent with Swider's[5] table 7d. A parameterization of cosmic ray ionization variation[7] gives an ionization constant of $3.0 \times 10^{-18}$ $molecules^{-1}$ $cm^3$ $sec^{-1}$. The latitude given in Sears[4] as the geomagnetic latitude appropriate for the eclipse data used is apparently the geographic latitude, and the appropriate geomagnetic latitude is 17.7° South.[8] Thus, the value used for the Galactic Cosmic Ray ionization constant is probably high for the ECLIPSE and low for the BENCHMARK runs. However, the data tabulated by Swider[5] indicate that this value of the ionization constant is not unreasonable.

The cosmic ray model makes no allowance for attenuation of the cosmic ray flux by the atmosphere, and therefore becomes increasingly inaccurate below 30 km.

---

[7] M. G. Heaps, "The Ion Pair Production Due to Cosmic Rays," BRL Memorandum Report 2641, June 1976. (AD #A027629)

[8] D. C. Baker, "Ionospheric D-Region Parameters from Blunt Probe Measurements during a Solar Eclipse," Scientific Report #334, pp. 45-46, Penn. State University, February 1, 1969.

The Precipitating Electron pair production model is based on that given by Sears.[4] In his appendix B, which is reproduced in Table 3 of the appendix, he gives the average pair production rate versus altitude for the South Atlantic anomaly at eclipse time. In his Figure 1 he also plots the maximum pair production rate, which is about 12 times greater. Both of these rates are based on extrapolations from trapped electron flux measurements made on September 30, 1966, some six weeks before the eclipse.

Sears' table gives data from 54 to 100 km only and the model was extended above 100 km by assuming that the pair production fell with a constant scale height above 98 km. The model was extended below 54 km by assuming that the scale height decreased at a constant rate below 58 km.

## ECLIPSE FUNCTIONS

One additional complication arises for the eclipse. The variation in energy input must be known if we are to accurately model the effects. Sears[4] gives several eclipse functions: for visible light he gives a table of values computed from the expression for a uniformly bright circular disc eclipsed by a disc of the same subtended angle -

$$Q = Q_o \, 2(\arcsin (t/d) + (t/d)(1 - (t/d)^2)^{1/2})/\pi$$

where

$Q_o \equiv$ the uneclipsed flux

$t \equiv$ time before or after totality

$d \equiv$ the semiduration of the eclipse.

This eclipse function is strictly true only in the far infrared.[9] For most wavelengths an optical depth of unity occurs below the temperature minimum in the solar atmosphere. Near the center of the solar disc the ray paths are vertical and the spectrum resembles that of a 6700 K black body.[10] Near the limb the ray paths are oblique, unity optical depth occurs at a higher, cooler altitude, and the effective radiation temperature is 5400K at the limb.[10] Sears' ultraviolet eclipse function, which reflects this limb darkening is given in Table 6 of the Appendix. For Lyman alpha the effects of limb darkening are counteracted by resonant scattering from the hydrogen in the solar corona and the geocorona and Sears recommends:

---

[9] G. Abetti, The Sun, Macmillan, N.Y., 1951, Fig. 85, p. 282.

[10] G. Abetti, *ibid.*, Fig. 86, p. 285.

$$Q_{Ly} = Q_{vis} + .001 \quad \text{for } t < 3400 \text{ seconds}$$

$$= Q_{vis} + .002 \quad \text{for } t < 1700 \text{ seconds.}$$

The x-ray flux originates to a large extent in the solar corona and is highly variable in space and time. Sears' recommended eclipse function is given in the Appendix (Table 6) and is quite asymmetric.

During totality the eclipse functions used were

$$Q_{visible} \equiv Q_{ultraviolet} \equiv 0.$$

$$Q_{Lyman\ alpha} \equiv (.001 + .001 * t/d')Q_o$$

where t ≡ time from the center of totality and d' ≡ the semiduration of totality. For x-rays we interpolated linearly between the values at 2nd contact (the start of totality) and 3rd contact (the end of totality).

We were strongly influenced by Abetti's[9] limb darkening curves when assigning our solar bands to these eclipse functions. We used the ultraviolet eclipse function for the near ultraviolet and throughout the visible (our bands 28-47, 174-740 nm). We used the Lyman alpha function for our bands 11-24, 100-148nm, and the "visible" eclipse function only for bands 25-27, 148-174 nm.

## ATMOSPHERIC ATTENUATION COMPUTATIONS

The solar model gives us the photon flux at the top of the atmosphere, but the information we need is the photon flux at some lower level where we are simulating the atmospheric chemistry. We model the atmospheric attenuation of the solar flux by Beer's Law

$$I = I_o e^{-N\sigma}$$

where $I_o$ ≡ initial photon flux in photons - $cm^{-2}$ - $sec^{-1}$

N ≡ line of sight number density per square centimeter

σ ≡ absorption cross section in square centimeters

I ≡ the attenuated photon flux one band at a time.

Because there are more than one absorbing species we replace Nσ by $\sum_i N_i \sigma_i$ to get

$$I = I_o e^{-\sum N_i \sigma_i}$$

Seven atmospheric species enter into the attenuation calculations: Argon, carbon dioxide, atomic and molecular nitrogen, atomic and molecular oxygen, and ozone. The absorption cross sections given in Table 1 of the Appendix were used both for the ECLIPSE[1] calculations and for the BENCHMARK[5] calculations. The x-ray cross sections are from Swider.[5] The cross sections for the other wavelengths can be found by looking for the same species in the lists of photolytic reactions in the Appendix.

The species number densities are the same as those used as initial data for the AIRCHEM[11] and BENCHMARK computations,[12] but the absorbing species density model has been extended from 0-500 km using the DNA reaction rate handbook DNA 1948H.[13] In some cases densities have been extrapolated beyond those given in the sources to avoid sudden jumps in the computed flux level for small changes in ray path.

The column densities of the absorbing species were found by integrating the column densities along the ray path from its lowest point until the OPTIR convergence criterion of a less than 1 percent change in the column density per integration step had been met for all absorbing species. The scale path length (i.e., the projection of the scale height on the ray path) was then computed for each absorbing species and was used to extrapolate the column density to the top of the atmosphere. The column densities were then checked again to ensure that either the extrapolated column density was less than .01 gm $cm^{-2}$ (i.e., negligible) or that the extrapolation caused an increase of less than 10 percent in the column density. If any species failed both of these criteria the OPTIR criterion was halved and integration along the ray path was resumed.

Two problems with the absorption computations must now be considered.

## I. Time Variation of Absorbing Species

In general the chemistry may cause the number density of an absorbing species to change with time. For the present case, only one absorbing species, ozone, changes enough to cause a problem. If the ray path

---

[11] E. L. Lortie, M. D. Kregel and F. E. Niles, "AIRCHEM: A Computational Technique for Modeling the Chemistry of the Atmosphere," BRL Report No. 1913, August 1976 (AD#A030157).

[12] F. E. Niles and J. M. Heimerl, "Selected Neutral Species Profiles 0-100 km," BRL Memo Report No. 2767, July 1977 (AD#A042620).

[13] DNA Reaction Rate Handbook, DNA 1948H, Chapter 2, Revision 1, DASIAC, GE-TEMPO, Santa Barbara, CA, 1972.

is nearly vertical so that most of the absorption occurs near the altitude of the chemical computations, and the species in question causes only a small amount of absorption, we may make the assumption that the variation in line of sight density is proportional to the variation in computed density. This assumption holds for the ECLIPSE[1] - the ray path was within 40° of vertical and the computations were for altitudes ≥ 60 km, well above the ozone maximum. For the BENCHMARK[2] runs the density of the absorbing ozone was held constant; the solar inputs were computed once for an overhead sun using the initial model densities. This assumption would not hold for ray paths which dipped below the ozone maximum, and would be grossly violated for sunrise/sunset studies.

## II. Choice of Effective Cross Sections

The relatively wide bands in our solar model lead to another problem. The cross sections of absorbing species can vary by several orders of magnitude over one of our bands, making our choice of the proper effective cross section difficult. A particularly severe problem is presented by the Schuman-Runge bands of molecular oxygen,[14] which roughly correspond to our bands 27-31 (167-210 nm). Oxygen also has a strongly varying cross section over our bands 13-17 and 19 (105-121 nm and 125-129 nm). For our band 18, which is dominated by Lyman alpha, we use cross sections for Lyman alpha. Parts of this discussion also apply to $N_2$ absorption, bands 11-23 (100-148 nm).

Fortunately, it can be shown[15,16] that the absorption due to an isolated gaussian line which is narrow with respect to the measuring instrument has an effective absorption cross section which varies inversely with the square root of the absorber density, and that this relationship holds provided the optical density at the peak of the line is at least unity. It can also be shown[17] that this relationship holds approximately for triangular lines, for randomly spaced arrays of lines, and for evenly spaced arrays of lines. This relationship has been experimentally verified by Blake *et al.*[15] for a range of absorption sufficient to vary the light intensity in the Schuman-Runge bands by two orders of magnitude.

---

[14] G. Kockarts, "Penetration of Solar Radiation in the Schuman-Runge Bands of Molecular Oxygen," in Mesospheric Models and Related Experiments, G. Fiacco, ed., Springer Verlag, N.Y., pp. 160-176.

[15] A. J. Blake, J. H. Carver, and G. N. Haddad, "Photoabsorption Cross Sections of Molecular Oxygen Between 1250Å and 2350Å," J. Quant. Spect. and Rad. Transfer 6, 453-454 (1966).

[16] J. R. Nielson, V. Thornton, and E. B. Dale, "Absorption Laws for Gases in the Infrared," Rev. Mod. Phys. 16, 307 (1944).

[17] A. E. S. Green and P. J. Wyatt, Atomic and Space Physics, Sections 8-3 and 8-4, pp. 410-429, Addison-Wesley, N.Y., 1968.

We now consider what cross sections to use for those bands for which the cross section varies too widely for one cross section to be suitable. We assume that the unattenuated photon flux is relatively constant across the band. We also assume that there is some reasonable distribution of cross sections between $\sigma_{max}$, the maximum cross section within the band, and $\sigma_{min}$, the minimum cross section. Consider dividing a band into sub-bands whose boundaries are defined by $\sigma_{max}$, $\sigma_{max/4}$, $\sigma_{max/16}$, $\cdots$, $4\sigma_{min}$, $\sigma_{min}$. We will accept a cross section distribution as reasonable if the sub-band intervals are approximately equal. If this is true

$$n = \frac{1}{1.4} \ell n(\sigma_{max}/\sigma_{min})$$

and $$1.4 = \ell n(4) \ .$$

Then when the number density of an absorber along the line of sight is less than $1/\sigma_{max}$ only the peaks are contributing to the absorption and

$$\sigma_e = 0.5 \ \sigma_{max}/n$$

where $\sigma_e \equiv$ the effective cross section, i.e., the one we should use in our absorption calculations. In other words, 1/2 of $\sigma_{max}$ is effective over 1/nth of our band or (1/2n)th of $\sigma_{max}$ is effective over the whole band.

Hudson[18] indicates that in much of the ultraviolet region the measured cross sections are instrumental bandwidth dependent, and that in general the peak cross sections should be greater and the minimum cross sections should be lower. We will therefore assume that for the most intense sub-band

$$\sigma_e = \sigma_{max}/n = 1.4 \ \sigma_{max}/\ell n(\sigma_{max}/\sigma_{min}) .$$

If the number density is such that $1/\sigma_{max} << N << 1/\sigma_{min}$ and if the inverse square law does hold, then $\sigma_e = \sigma_0 \ N_0^{1/2}/N^{1/2}$ where $N_0$ is the line of sight density when $\sigma_e = \sigma_0$. If we let $\sigma_0 = \sigma_e$ when $N = 1/\sigma_{max}$

$$\sigma_e = \sigma_{max} \cdot 1.4/(\ell n(\sigma_{max}/\sigma_{min})(\sigma_{max} \ N)^{1/2})$$

$$= 1.4 \ \sigma_{max}^{1/2}/(N^{1/2} \ \ell n(\sigma_{max}/\sigma_{min})) \ .$$

---

[18] R. D. Hudson, " Review of UV Cross Sections," Rev. Geophys. and Space Phys. 9, No. 2, 304-406 (1971).

If the number density is very large then $N >> 1/\sigma_{min}$ and $\sigma_e \geq \sigma_{min}$. We now have 3 expressions; it would be simpler if we only had one.

Clearly, we can combine the latter two cases by simple addition to get

$$\sigma_e = 1.4\ (\sigma_{max}/N)^{\frac{1}{2}}/\ell n(\sigma_{max}/\sigma_{min}) + \sigma_{min}$$

for all $N >> 1/\sigma_{max}$.

Similarly, we can combine the first two cases by taking the harmonic sum $1/S = 1/a + 1/b$.

If we let $$a = 1.4\ \sigma_{max}/\ell n(\sigma_{max}/\sigma_{min})$$

$$b = 1.4\ \sigma_{max}^{\frac{1}{2}} N^{-\frac{1}{2}}/\ell n(\sigma_{max}/\sigma_{min})$$

and $S = \sigma_e$ ,

then

$$\sigma_e = 1.4\ \sigma_{max}/(\ell n(\sigma_{max}/\sigma_{min})(\sigma_{max}^{\frac{1}{2}} N^{\frac{1}{2}} + 1))$$

for $N < 1/\sigma_{min}$.

Since $\sigma_e = \sigma_{min}$ for $N > 1/\sigma_{min}$ we can add this to get

$$\sigma_e = \sigma_{min} + 1.4\ \sigma_{max}/(\ell n(\sigma_{max}/\sigma_{min})(\sigma_{max}^{\frac{1}{2}} N^{\frac{1}{2}} + 1))$$

for all absorption calculations.

Because we now have two cross sections, $\sigma_{max}$ and $\sigma_{min}$, rather than one for some bands we now have a minor storage and retrieval problem. For $O_2$, and only for those bands where the problem existed, $\sigma_{max}$ was stored as an absorption cross section and $\sigma_{min}$ as a dissociation cross section. For $N_2$, $\sigma_{max}$ was stored as an absorption cross section and $\sigma_{min}$ was set to $3 \times 10^{-24}$ $cm^2$.

For $CO_2$ there is a different problem. The $CO_2$ absorption cross section decreases rapidly with increasing wavelength across the $O_2$ Schuman-Runge bands. The $O_2$ absorption is greater and strongly modulates the solar source seen by the $CO_2$. The effective $CO_2$ absorption is therefore also modulated by the $O_2$ absorption. To simulate this modulation, the $CO_2$ cross section was made to vary by the same proportion of its range between $\sigma_{max}$ and $\sigma_{min}$ that the $O_2$ cross section did. Because the $CO_2$ cross section was decreasing monotomically with

increasing wavelength, $\sigma_{min}$ for band n could be set to $\sigma_{max}$ for band n+1 and so $\sigma_{max}$ was stored for each band.

Note that these attempts to allow for square root low absorption result in some cross sections for $O_2$, $N_2$, and $CO_2$ which seem to have unusually high or low values.

Because of an algebraic error the factor 1.4 in the final expression for the cross section was replaced by a 2 in the computer program. The effect of this error will be discussed in the section on photolytic reactions.

Atmospheric attenuation of the precipitating electron flux is included in the model. Atmospheric attenuation of the galactic cosmic ray flux is small above 30 to 35 kilometers and the effects of attenuation are therefore ignored.

## PHOTOLYTIC REACTIONS

These are reactions which are driven by photons and which decompose a chemical substance. The rate constants of the photolytic reactions are computed using the expression

$$R_n = \sum_j \sigma_{nj} I_j$$

where

$n \equiv$ reaction number

$j \equiv$ wavelength band number

$R_n \equiv$ reaction rate constant

$\sigma_{nj} \equiv$ reaction and band specific cross section

$I_j \equiv$ attenuated photon flux.

The reactions, cross sections and references for the ECLIPSE study[1] are listed in Tables 4 and 5 of the Appendix, and those for the BENCHMARK study[2] are listed in Tables 7 and 8 of the Appendix.

Because the various ionizing mechanisms differ mainly in their energy sources we have been able to reduce the number of chemical reactions. Ionization by Energetic Particles can be described by chemical equations which are formally the same as the equivalent photo-ionization reaction equations. These equivalent reactions were combined and the rate constant for each combined reaction was obtained by adding those of its constituent reactions. For example, there is only one ionization reaction for molecular oxygen

$$O_2 + h\nu \rightarrow O_2^+ + e$$

with

$$R_n = R_{uv} + R_x + R_{phe} + R_{pre} + R_{gcr}$$

where

$h\nu \equiv$ photons from all ionization sources

$R \equiv$ reaction rate constant

$n \equiv$ reaction number

$uv \equiv$ ultraviolet

$x \equiv$ x-rays (primary ionization only)

$phe \equiv$ photo-electrons

$pre \equiv$ precipitated electrons

$gcr \equiv$ galactic cosmic rays

The ionization due to energetic particles was computed by first adding the pair production rates of the source models of galactic cosmic rays, photo electrons, and precipitated electrons and then dividing this pair production among the atmospheric species. Following Swider[5] we assumed that the cross section of an oxygen atom was 1.15 times that of a nitrogen atom, that the cross sections of molecules were stoichiometric multiples of the cross sections of their constituent atoms, and that these ratios were approximately valid for all three sources. We also chose to ignore all atomic species except Nitrogen and Oxygen.

Then

$$\text{Pairs}_{total} = \text{Pairs}_{gcr} + \text{Pairs}_{phe} + \text{Pairs}_{pre}$$

and

$$R'_n = \frac{\langle N \rangle + 1.15 \langle O \rangle}{[N] + 1.15 [O]} \text{Pairs}_{Total}$$

where $\text{Pairs}_{total}$ = total pair production rate

$gcr$ = galactic cosmic rays

$phe$ = photo-electrons and multiply charged ions

$pre$ = precipitating electrons

$R'_n$ = ionization rate constant for species n by particles

< > indicates the number of N and O atoms in species n.

[ ] indicates the total local atomic number density of N or O.

Dyadichov and Kozlov[19] give values for relative production rates and branching ratios which corroborate those given by Swider.[5] The major difference is in the relative cross sections for photoelectron ionization. Dyadichov and Kozlov give cross sectional ratios of O: $O_2$ : $N_2$ = 0.56 : 1.5 : 1.15, while Swider gives O : $O_2$ : $N_2$ = 0.575 : 1.15 : 1.0, the ratios used in these studies.

Dyadichov and Kozlov[19] also indicate that the photoelectron ionization of $N_2$ is accompanied by dissociation reactions with rates amounting to 40% - 90% of the ionization rate. They further indicate that all of the N produced by dissociative ionization and 75% of the N produced by dissociation by photoelectrons is $N(^2D)$. In the code, the computed value for $N(^2D)$ is expected to be low because these reactions forming $N(^2D)$ were not included.

Dissociative Ionization was included only for the two species $N_2$ and $O_2$, whose branching ratios[5] are 0.19 and 0.29, respectively. Similar branching ratios were found by Dyadichov and Kozlov.[19]

Predissociation is a reaction path which includes a molecule absorbing energy, being raised to an excited state, switching to another excited state, and then dissociating. This takes time, and radiation or collisional quenching are possible alternate paths. The branching ratio between radiation and predissociation is constant, but the collisional quenching rate is a function of M, the local number density, and hence is a strong function of altitude. Ideally this would be modelled by including a metastable species and the several decay paths. Because the reaction set was already large, the rates for the alternate paths were not well known, and these paths were only important for their effect on the dissociation path, we modelled predissociation by chosing a quantum efficiency, $\phi$, which seemed reasonable over the altitude range of interest. For $N_2$ we chose a $\phi$ of zero because the rate is very slow[20] and is only effective at high altitudes. For NO we chose a $\phi$ of unity[21] for our bands < 28, $\lambda$ < 190 nm. For $O_2$ we chose a $\phi$ of one half[22] for our bands

---

[19] V. N. Dyadichov and S. I. Kozlov, "Minor Ion Components in the Disturbed Ionosphere in the Altitude Range 100-200 km," Cosmic Res. 13, No. 2, 218-218 (1975).

[20] P. M. Banks and G. Kockarts, Aeronomy, Part A, Academic Press, N.Y., 1973, p. 176 and p. 318.

[21] S. Cieslik and M. Nicolet, "The Aeronomic Dissociation of Nitric Oxide," Planet. Space Sci. 21, 925-938 (1973).

[22] M. Ackerman, F. Biaumé and G. Kockarts, "Absorption Cross Sections of the Schuman-Runge Bands of Molecular Oxygen," Planet. Space Sci. 18, 1639-1651 (1970).

27-29 (167-190 nm) and a $\phi$ of zero for our bands > 29 ($\lambda$ > 190 nm) which corresponds to predissociation for v' > 3 in the Schuman-Runge bands.[23] For our bands < 27 the value of $\phi$ was absorbed into $\sigma$. The resulting $O_2$ dissociation had an altitude variation which agreed well with that given by Banks and Kockarts.[23]

## PHOTOLYTIC CROSS SECTIONS

The cross sections used in computing the photolytic reaction rate constants were chosen at times when our knowledge of negative ion cross sections was changing rapidly and hindsight indicates that some guesses and extrapolations from private communications were more fortunate than others. Several of the less fortunate choices and some other problems which arose in choosing cross sections will now be discussed. Reaction numbers without parentheses refer to the ECLIPSE[1] reaction set and will be found with their references in Tables 4 and 5 of the Appendix. Reaction numbers within parentheses refer to the BENCHMARK[2] reaction set and will be found with their references in Tables 7 and 8 of the Appendix. The actual rate constants computed for BENCHMARK are shown in Table 9 of the Appendix.

For the reaction:

$$NO_2^- \rightarrow NO_2 + e \qquad 3\ (1)^{\dagger}$$

a zero shift seems to have occurred in the conversion from $cm^{-1}$ to band number. The cross sections are correct for the next, numerically higher band number. In effect, the cutoff has been shifted to a 10% shorter wavelength. The solar flux increases strongly in the cutoff region, so that the reaction rate constant was reduced by one third, and the rate constants for reaction (1)3, in Table 9 should be increased by 50% to obtain the correct value. We based our cross sections on those computed by Herbst *et al.*[24] for a vibrational temperature of 250 K. We did not use their measured cross sections because these were estimated to correspond to an effective temperature of 1750 K.[24] Use of the measured (1750 K) cross sections would increase the rate constants for Reaction 3(1) by an additional 20%. Herbst *et al.* did not include rotation effects in their cross section calculations. This neglect of rotation should be equivalent to lowering the effective temperature by an insignificant amount.

Herbst *et al.*[24] also measured a photodissociation cross section for the peroxy isomer of $NO_2^-$. This species is not in our reaction set, but

---

[23] P. M. Banks and G. Kockarts, Aeronomy, Part A, 167-174, Academic Press, N.Y., 1973.

[24] E. Herbst, T. A. Patterson, and W. C. Lineberger, "Laser Photodetachment of $NO_2^-$," J. Chem. Phys. 61, No. 5, 1300-1304 (1974).

† Read as Reaction 3 of ECLIPSE studies and Reaction 1 of BENCHMARK studies.

could be important[25,26] because the photodissociation rate for

$$NO_2^{-*} + h\nu \rightarrow NO + O^- \qquad 3a\ (1a)$$

would be twice the corrected rate constant for Reaction 3(1). One possible production path for $NO_2^{-*}$ is the reaction[25]

$$CO_3^- + NO \rightarrow NO_2^{-*} + CO_2.$$

For the reaction

$$CO_3^- + h\nu \rightarrow CO_2 + O^-, \qquad 7(6)$$

later measurements and estimates by Peterson[26] give values of $\sigma$ which vary from 135% of our $\sigma$ at longer wavelengths to 0.0% at shorter wavelengths. The net effect is that our computed rate constants are 7-9% higher than they would have been if we had used Peterson's[26] cross sections.

For the reaction

$$CO_3^-(H_2O) + h\nu \rightarrow CO_3^- + H_2O, \qquad 8(7)$$

we used a constant 10 megabarn ($10^{-17}$ cm$^2$) cross section throughout the visible ultraviolet wavelength range. Peterson[26] gives cross sections which are lower by 50% in the longest wavelength band, lower by 75-80% between 400 and 520 nm, and zero cm$^2$ for $\lambda < 390$ nm. From Peterson's cross sections we would compute a rate constant for reaction 8(7) which is about 45% lower than the rate constants which we obtained from the cross sections we did use.

For the reaction

$$NO_3^{-*} + h\nu \rightarrow NO + O_2^- \qquad 12(12)$$

we used the same shape at cutoff as for the reaction

$$NO_3^- + h\nu \rightarrow NO_2 + O + e^- \qquad 4(11)$$

Because the solar photon flux decreases much more rapidly at the shorter wavelengths where the $NO_3^-$, 4(11), and $NO_3^{-*}$, 12(12), photodissociation reactions cut off than it does at the longer wavelengths where the $NO_2^-$, 3(1), and $NO_2^{-*}$, 3a(1a), reactions cut off, the difference between

---

[25] J. H. Richardson, L. M. Stephenson, and J. I. Brauman, "Photodetachment of $NO_2^{-*}$, Experimental Evidence for a New Isomer," Chem. Phys. Lett. 25, No. 2, 318-320 (1974).

[26] J. R. Peterson, "Sunlight Photodestruction of $CO_3^-$, $CO_3^- \cdot H_2O$, and $O_3^-$: The Importance of Photodissociation to the D-Region Electron Densities at Sunrise," J. Geophys. Res. 81, 1433-1435 (1976).

the rate constants is much greater for the former reactions than for the latter reactions.

The effects of these changes to the rate constants in Table 9 of the Appendix are shown in Table 2.

Positive Ion Reactions

Positive ion photolytic reactions were formally included in the BENCHMARK-76 reaction set in Table 9 of the Appendix as reactions 18-32 but in practice the rate constants were set to zero. They were not included in the ECLIPSE-66 reaction set.

Neutral Species Reactions

The square root law variation in the absorption cross section of $O_2$ which is discussed under attenuation computations is also reflected in the $O_2$ dissociation cross sections. For normal, Beer's law absorption

$$I = I_o\, e^{n\sigma}$$

and

$$dI/dN = - I_o\, \sigma e^{-n\sigma}$$

where $\sigma$ is a constant. But, for square root law absorption

$$\sigma = \sigma_o\, (N_o/N)^{1/2}$$

and

$$dI/dN = - 1/2\ I_o \sigma e^{-n\sigma}$$

so that the effective cross section for the dissociation calculations is 1/2 of the effective cross section for the attenuation calculations. With this change the expression for the effective cross section for $O_2$ dissociation in the square root law region becomes

$$\sigma_e = 1.4\ \sigma_{max}/(\ell n(\sigma_{max}/\sigma_{min})(1 + 2N\ \sigma_{max})^{1/2}) + \sigma_{min}$$

for all N.

Again, due to an algebraic error, the factor 2.0 rather than 1.4 was used in the actual computations. For $O_2$ this would tend to compensate for an identical error in the attenuation calculations. The absorption cross section error raises the altitude at which absorption occurs by 2-4 kilometers. The dissociation cross section error raises the contribution of the affected bands by 50%. For $O_2$ the latter effect would predominate above the altitude of unit optical depth and the former effect below that altitude.

TABLE 2. REVISED REACTION RATE CONSTANTS ($s^{-1}$)

| Remarks | Reaction No. | Altitude in km 80 | 70 | 60 | 50 | 40 | 30 | 20 | 10 |
|---|---|---|---|---|---|---|---|---|---|
| 250 K $NO_2^-$ cross sections of ref. 24 | 3 (1) | .0524 | .0524 | .0524 | .0522 | .0511 | .0488 | .0488 | .0485 |
| 250 K $NO_2^{-*}$ cross sections of ref. 24 | 3a (1a) | .107 | .107 | .107 | .107 | .105 | .102 | .100 | .100 |
| 1500 K $NO_2^-$ cross sections of ref. 24 | 3b (1b) | .0623 | .0623 | .0622 | .0620 | .0609 | .0595 | .0585 | .0582 |
| 1500 K $CO_3^-$ cross sections of ref. 26 | 7 (6) | .196 | .196 | .196 | .196 | .196 | .195 | .193 | .192 |
| 1500 K $CO_3^-(H_2O)$ cross sections of ref. 26 | 8 (7) | 1.089 | 1.089 | 1.089 | 1.089 | 1.089 | 1.085 | 1.074 | 1.066 |

Effects similar to the interaction between the $O_2$ absorption cross section and the $CO_2$ absorption cross section in the Schuman-Runge region, our solar bands 27-31 (167-210 nm), should now be considered. Both $CO_2$ and $H_2O$ have photodissociation cross sections which decrease very strongly with increasing wavelength in this region. Therefore for the two photodissociation reactions

$$CO_2 + h\nu \rightarrow CO + O \qquad 16\ (-)^{\dagger}$$

$$H_2O + h\nu \rightarrow H + HO \qquad 30\ (34)$$

we made adjustments in the photodissociation cross section identical to the adjustment in the $CO_2$ absorption cross section which was discussed under atmospheric attenuation calculations.

The solar flux is increasing moderately with increasing wavelength at the same time that the $O_2$ absorption cross section is decreasing, an effect which partially offsets the cross section interactions. A correction similar to the cross section correction was applied to the photon flux for the ECLIPSE 66 study.[1] It overcompensated at low absorption and was not used for BENCHMARK 76.[2]

The X-Ray Ionization Cross Sections for the species N, $N_2$, NO, $NO_2$, O, $O_2$ and $O_2(^1\Delta)$ were computed from the $N_2$ and $O_2$ X-ray absorption cross sections using the formula

$$\sigma_{ij} = .5 \langle N \rangle \sigma_{N_2 j} + .5 \langle O \rangle \sigma_{O_2 j}$$

where

$\sigma$ is the cross section

i is the reaction number

j is the solar band number

$\langle\ \rangle$ refers to the number of atoms of N or O in the species.

The cross section for ionization of $O_2$ by solar Lyman $\beta$ was set at $1.6 \times 10^{-22}$ $m^2$ rather than $1.0 \times 10^{-22}$ $m^2$.[3] This would have a maximum effect at 100 km where the total solar ionization rate was 25% high, but the effect was less than 1/2% at 90 km and negligible below that height.

---

[†]This reaction was not in the BENCHMARK-76 set because CO was not included in the species set.

## COMMENTS ON THE CALCULATIONS

Atmospheric chemistry models are frequently allowed to run for several model weeks to eliminate all start up transients.[11] The AIRCHEM models were designed to study the reaction of the atmosphere to ionization shocks. They are zero dimensional, transportless, and make no claim to model slow chemistry. For the ECLIPSE-66[1] study we turned the sun on at 10 AM model time and let the program run till 2 PM model time. The 2 PM ion densities were used as initial densities for a second run starting at 10 AM. The new 2 PM ion densities were then used as initial densities for a third run with the ECLIPSE turned on. The 10:30 AM model densities usually agreed to better than 2-5% and the 2 PM densities for the first and second days agreed to a few tenths of a percent. The neutral densities stayed within their estimated error bars except for $N(^2D)$. This density fell to zero because several formation reactions were not considered.[19] (See above for findings of Dyadichov and Kozlov.) For the ECLIPSE-66[1] study the SOURCE package was called to update the reaction rate constants at both the prediction and correction stages in the integrator.[11] For the BENCHMARK-76 study[2] the package stood alone, and the initial neutral density model[12] was used to compute the rate constants, which are given in Table 9 of the Appendix, and which also appears as Table 3 of reference 2(I). The atmospheric temperature model was taken from the WEPH 4 code.[27]

---

[27] W. S. Knapp, R. L. Bogusch, M. I. Chock, "A FORTRAN Code for the Calculation of Ionization and Absorption Due to a Nuclear Detonation (WEPH 4)," GE-TEMPO, 68 TMP-44, DASA 2096, 30 April 1968.

## REFERENCES


1. F. E. Niles and I. L. Chidsey, "Comparison of Measured and Calculated D-Region Electron Density for Solar Eclipse of 12 November 1966," and I. L. Chidsey and F. E. Niles, "Comparison of Measured and Calculated D-Region Positive-Ion Number Density for Solar Eclipse of 12 November 1966," Trans. AGU 56, 997 (1975).

2. J. M. Heimerl and F. E. Niles, "BENCHMARK-76 Model Computations for Disturbed Atmospheric Conditions, I. Input Parameters," BRL Report No. 2022, October 1977; "BENCHMARK-76 Model Computations for Disturbed Atmospheric Conditions, II. Results for the Stratosphere and Mesosphere," BRL Report ARBRL-TR-02050, March 1978; and "BENCHMARK-76 Model Computations for Disturbed Atmospheric Conditions, III. Results for Selected Excitation Parameters at 60 km," BRL Report ARBRL-TR-02051, April 1978. (AD Nos. A050355, A054325, and A054376)

3. O. P. Manley, H. J. P. Smith, Y. M. Treve, J. W. Carpenter, T. C. Degges, and L. R. Doone, "OPTIR II," AFCRL-71-0528 (1), AFCRL, Bedford, MA, 1971.

4. R. D. Sears, "Analysis of the 1966 Solar Eclipse Data," LMSC D246526, Lockheed Palo Alto Research Lab, Palo Alto, CA, 1972.

5. W. Swider, Jr., "Ionization Rates Due to the Attenuation of 1-100Å Nonflare Solar X-Rays," Rev. Geophys. 7, No. 3, 573-594 (August 1969).

6. M. Ackerman, "Ultraviolet Solar Radiation Related to Mesospheric Processes," in Mesospheric Models and Related Experiments, G. Fiacco, ed., Springer Verlag, N.Y., 149-159 (1971).

7. M. G. Heaps, "The Ion Pair Production Due to Cosmic Rays," BRL Memorandum Report 2641, June 1976.

8. D. C. Baker, "Ionospheric D-Region Parameters from Blunt Probe Measurements during a Solar Eclipse," Scientific Report #334, pp. 45-46, Penn. State University, February 1, 1969.

9. G. Abetti, The Sun, Macmillan, N. Y., 1951, Fig. 85, p. 282.

10. G. Abetti, *ibid.*, Fig. 86, p. 285.

11. E. L. Lortie, M. D. Kregel and F. E. Niles, "AIRCHEM: A Computational Technique for Modeling the Chemistry of the Atmosphere," BRL Report No. 1913, August 1976 (AD#A030157).

12. F. E. Niles and J. M. Heimerl, "Selected Neutral Species Profiles 0-100 km," BRL Memo Report No. 2767, July 1977 (AD#A042620).

13. DNA Reaction Rate Handbook, DNA 1948H, Chapter 2, Revision 1, DASIAC, GE-TEMPO, Santa Barbara, CA, 1972.

14. G. Kockarts, "Penetration of Solar Radiation in the Schuman-Runge Bands of Molecular Oxygen," in Mesospheric Models and Related Experiments, G. Fiacco, ed., Springer Verlag, N.Y., pp. 160-176.

15. A. J. Blake, J. H. Carver, and G. N. Haddad, "Photoabsorption Cross Sections of Molecular Oxygen Between 1250Å and 2350Å," J. Quant. Spect. and Rad. Transfer 6, 453-454 (1966).

16. J. R. Nielson, V. Thornton, and E. B. Dale, "Absorption Laws for Gases in the Infrared," Rev. Mod. Phys. 16, 307 (1944).

17. A. E. S. Green and P. J. Wyatt, Atomic and Space Physics, Sections 8-3 and 8-4, pp. 410-429, Addison-Wesley, N.Y., 1968.

18. R. D. Hudson, " Review of UV Cross Sections," Rev. Geophys. and Space Phys. 9, No. 2, 304-406 (1971).

19. V. N. Dyadichov and S. I. Kozlov, "Minor Ion Components in the Disturbed Ionosphere in the Altitude Range 100-200 km," Cosmic Res. 13, No. 2, 218-218 (1975).

20. P. M. Banks and G. Kockarts, Aeronomy, Part A, Academic Press, N.Y., 1973, p. 176 and p. 318.

21. S. Cieslik and M. Nicolet, "The Aeronomic Dissociation of Nitric Oxide," Planet. Space Sci. 21, 925-938 (1973).

22. M. Ackerman, F. Biaumé and G. Kockarts, "Absorption Cross Sections of the Schuman-Runge Bands of Molecular Oxygen," Planet. Space Sci. 18, 1639-1651 (1970).

23. P. M. Banks and G. Kockarts, Aeronomy, Part A, 167-174, Academic Press, N.Y., 1973.

24. E. Herbst, T. A. Patterson, and W. C. Lineberger, "Laser Photodetachment of $NO_2^-$," J. Chem. Phys. 61, No. 5, 1300-1304 (1974).

25. J. H. Richardson, L. M. Stephenson, and J. I. Brauman, "Photodetachment of $NO_2^{-*}$, Experimental Evidence for a New Isomer," Chem. Phys. Lett. 25, No. 2, 318-320 (1974).

26. J. R. Peterson, "Sunlight Photodestruction of $CO_3^-$, $CO_3^- \cdot H_2O$, and $O_3^-$: The Importance of Photodissociation to the D-Region Electron Densities at Sunrise," J. Geophys. Res. 81, 1433-1435 (1976).

27. W. S. Knapp, R. L. Bogusch, M. I. Chock, "A FORTRAN Code for the Calculation of Ionization and Absorption Due to a Nuclear Detonation (WEPH 4)," GE-TEMPO, 68 TMP-44, DASA 2096, 30 April 1968.

## APPENDIX

This appendix contains several tables of input data used in the ECLIPSE-66 and BENCHMARK-76 studies, and also, as a sample output the table of quiescent production rates used in the BENCHMARK study. Tables A1 through A3 apply to both studies; the other tables apply to only one study as noted.

Table A1 lists for each band in the solar model, the band limits in millimicrons ($10^{-9}$ m), the absorption cross sections of the absorbing species, the solar flux in photons $cm^{-2}$ $sec^{-1}$, and the model band number.

Table A2 lists for bands 11-20 the ultra-violet ionization cross sections in megabarns ($10^{-22}$ $M^2$) for the species NO, $NO_2$, $O_2$, $O_2(^1\Delta)$ versus band number.

Table A3 lists the electron precipitation model[4] in ion pairs $cm^{-3}$ $s^{-1}$ versus altitude in km.

Table A4 lists for bands 11-47 the photodetachment and photodissociation cross sections in $cm^{-2}$ for reactions 1-37 in the ECLIPSE-66 model.

Table A5 lists for all bands and photolytic reactions the references for the ECLIPSE-66 model.

Table A6 lists the uv and x-ray eclipse functions[4] used in the ECLIPSE-66 model.

Table A7 lists for bands 11-47 the photodetachment and photodissociation cross sections in $cm^{-2}$ for reactions 1-49 in the BENCHMARK-76 model.

Table A8 lists for all bands and photolytic reactions the references for the BENCHMARK-76 model.

Table A9 lists the quiescent production rates derived from the above mentioned data for the BENCHMARK-76 model.

TABLE A1. ABSORPTION CROSS SECTIONS AND SOLAR FLUX MODEL FOR ECLIPSE-66 AND BENCHMARK-76.

| WAVELENGTH NANOMETERS | | PHOTO-ABSORPTION CROSSECTIONS ( CM-2 ) SPECIES | | | | | SOLAR FLUX PHOTONS/CM2-SEC | SOLAR MODEL BAND NO. |
|---|---|---|---|---|---|---|---|---|
| FROM | TO | A | CO2 | N2 | O2 | O3 | | |
| .4 | .5 | 2.000E-20 | 0. | 1.100E-20 | 1.900E-20 | 2.800E-20 | 9.600E+03 | 1 |
| .5 | .8 | 5.000E-20 | 0. | 2.900E-20 | 5.000E-20 | 7.400E-20 | 7.600E+04 | 2 |
| .8 | 1.0 | 1.000E-19 | 0. | 6.000E-20 | 9.900E-20 | 1.500E-19 | 4.500E+05 | 3 |
| 1.0 | 3.1 | 2.410E-18 | 0. | 9.600E-20 | 1.640E-19 | 2.460E-19 | 1.200E+08 | 4 |
| 3.1 | 4.0 | 3.000E-18 | 0. | 1.810E-19 | 3.080E-19 | 4.620E-19 | 1.900E+08 | 5 |
| 4.0 | 5.0 | 3.700E-19 | 0. | 2.980E-19 | 5.090E-19 | 7.630E-19 | 3.700E+08 | 6 |
| 5.0 | 6.0 | 4.900E-19 | 0. | 4.530E-19 | 7.730E-19 | 1.160E-18 | 4.000E+08 | 7 |
| 6.0 | 7.0 | 6.300E-19 | 0. | 6.480E-19 | 1.100E-18 | 1.650E-18 | 4.000E+08 | 8 |
| 7.0 | 8.0 | 7.800E-19 | 0. | 8.850E-19 | 1.510E-18 | 2.270E-18 | 6.000E+08 | 9 |
| 8.0 | 9.0 | 9.500E-19 | 0. | 1.170E-18 | 2.000E-18 | 3.000E-18 | 7.000E+08 | 10 |
| 9.0 | 10.0 | 0. | 4.400E-17 | 3.000E-22 | 1.400E-18 | 1.000E-18 | 4.590E+09 | 11 |
| 100.0 | 102.6 | 0. | 1.800E-17 | 3.000E-22 | 1.000E-18 | 1.000E-18 | 2.620E+09 | 12 |
| 102.6 | 105.3 | 0. | 1.000E-17 | 3.000E-22 | 3.700E-18 | 9.300E-18 | 2.860E+09 | 13 |
| 105.3 | 108.1 | 0. | 1.100E-17 | 3.000E-22 | 2.900E-18 | 9.300E-18 | 2.000E+09 | 14 |
| 108.1 | 111.1 | 0. | 5.000E-17 | 3.000E-22 | 3.000E-18 | 1.040E-17 | 2.590E+09 | 15 |
| 111.1 | 114.3 | 0. | 1.500E-18 | 3.000E-22 | 7.000E-18 | 6.700E-18 | 1.300E+10 | 16 |
| 114.3 | 117.6 | 0. | 4.000E-20 | 3.000E-22 | 1.500E-17 | 9.300E-18 | 4.280E+09 | 17 |
| 117.6 | 121.2 | 0. | 1.300E-19 | 3.000E-22 | 1.000E-20 | 1.500E-17 | 2.750E+11 | 18 |
| 121.2 | 125.0 | 0. | 4.000E-19 | 3.000E-22 | 1.500E-18 | 7.100E-18 | 8.250E+09 | 19 |
| 125.0 | 129.0 | 0. | 8.000E-19 | 3.000E-22 | 1.000E-18 | 1.300E-17 | 1.110E+10 | 20 |
| 129.0 | 133.3 | 0. | 9.000E-19 | 3.000E-22 | 6.000E-18 | 9.300E-18 | 1.630E+10 | 21 |
| 133.3 | 137.9 | 0. | 8.000E-19 | 3.000E-22 | 1.400E-17 | 7.400E-18 | 1.900E+10 | 22 |
| 137.9 | 142.9 | 0. | 9.000E-19 | 3.000E-22 | 1.400E-17 | 5.600E-18 | 4.200E+10 | 23 |
| 142.9 | 148.1 | 0. | 7.000E-19 | 0. | 1.200E-17 | 3.300E-18 | 1.110E+11 | 24 |
| 148.1 | 153.8 | 0. | 4.000E-19 | 0. | 8.000E-18 | 1.120E-18 | 2.260E+11 | 25 |
| 153.8 | 160.0 | 0. | 1.500E-19 | 0. | 3.500E-18 | 9.300E-19 | 4.770E+11 | 26 |
| 160.0 | 166.7 | 0. | 2.700E-20 | 0. | 1.700E-18 | 8.200E-19 | 1.060E+12 | 27 |
| 166.7 | 173.9 | 0. | 4.000E-21 | 0. | 2.300E-18 | 7.400E-19 | 2.240E+12 | 28 |
| 173.9 | 181.8 | 0. | 4.000E-22 | 0. | 5.000E-19 | 6.700E-19 | 5.180E+12 | 29 |
| 181.8 | 190.5 | 0. | 1.500E-23 | 0. | 2.000E-20 | 4.100E-19 | 1.050E+13 | 30 |
| 190.5 | 200.0 | 0. | 3.000E-24 | 0. | 1.700E-22 | 3.300E-19 | 2.190E+13 | 31 |
| 200.0 | 210.5 | 0. | 2.000E-24 | 0. | 1.000E-23 | 1.100E-18 | 6.420E+13 | 32 |
| 210.5 | 222.2 | 0. | 0. | 0. | 5.000E-24 | 4.000E-18 | 1.040E+14 | 33 |
| 222.2 | 235.3 | 0. | 0. | 0. | 1.000E-24 | 9.200E-18 | 1.300E+14 | 34 |
| 235.3 | 250.0 | 0. | 0. | 0. | 0. | 1.100E-17 | 2.950E+14 | 35 |
| 250.0 | 266.7 | 0. | 0. | 0. | 0. | 5.600E-18 | 6.840E+14 | 36 |
| 266.7 | 285.7 | 0. | 0. | 0. | 0. | 6.000E-19 | 1.950E+15 | 37 |
| 285.7 | 307.7 | 0. | 0. | 0. | 0. | 2.000E-20 | 3.770E+15 | 38 |
| 307.7 | 333.3 | 0. | 0. | 0. | 0. | 1.000E-21 | 6.140E+15 | 39 |
| 333.3 | 363.6 | 0. | 0. | 0. | 0. | 0. | 8.680E+15 | 40 |
| 363.6 | 400.0 | 0. | 0. | 0. | 0. | 4.140E-23 | 1.145E+16 | 41 |
| 400.0 | 430.0 | 0. | 0. | 0. | 0. | 1.920E-22 | 1.851E+16 | 42 |
| 430.0 | 470.0 | 0. | 0. | 0. | 0. | 8.780E-22 | 2.015E+16 | 43 |
| 470.0 | 510.0 | 0. | 0. | 0. | 0. | 2.480E-21 | 2.581E+16 | 44 |
| 510.0 | 560.0 | 0. | 0. | 0. | 0. | 4.250E-21 | 3.237E+16 | 45 |
| 560.0 | 620.0 | 0. | 0. | 0. | 0. | 2.650E-21 | 3.040E+16 | 46 |
| 620.0 | 680.0 | 0. | 0. | 0. | 0. | 8.900E-22 | 3.524E+16 | 47 |
| 680.0 | 730.0 | 0. | 0. | 0. | 0. | | | |

TABLE A2. ULTRAVIOLET IONIZATION CROSS SECTIONS FOR ECLIPSE-66 AND BENCHMARK-76

| SPECIES | NO | $NO_2$ | $O_2$ | $O_2(^1\Delta)$ |
|---|---|---|---|---|
| ECLIPSE REACTION NO. | 39 | 40 | 42 | 43 |
| BENCHMARK REACTION NO. | 51 | 52 | 57 | 60 |
| BAND NO. | | | | |
| 11 | 14. | 3. | 1.6* | 5. |
| 12 | 8.5 | 3. | 0. | 5. |
| 13 | 6. | 3. | 0. | 4. |
| 14 | 4.8 | 3. | 0. | 3. |
| 15 | 3.2 | 1.6 | 0. | 0.7 |
| 16 | 2.4 | 0.4 | 0. | 0. |
| 17 | 2.1 | 0.12 | 0. | 0. |
| 18 | 1.9 | 0.06 | 0. | 0. |
| 19 | 1.3 | 0.004 | 0. | 0. |
| 20 | 0.7 | 0. | 0. | 0. |

*This was apparently a misprint which occurred when the program was key punched. $1.0 \times 10^{22}$ meters$^2$ is the value indicated by the reference.

TABLE A3. ELECTRON PRECIPITATION MODEL FOR ECLIPSE-66 AND BENCHMARK-76

| Altitude (km) | Pair Production Rate (ion-pairs $cm^{-3}$ $s^{-1}$) |
|---|---|
| 100 | .0047 |
| 98 | .0060 |
| 96 | .0077 |
| 94 | .0097 |
| 92 | .012 |
| 90 | .016 |
| 88 | .020 |
| 86 | .026 |
| 84 | .033 |
| 82 | .042 |
| 80 | .050 |
| 78 | .057 |
| 76 | .062 |
| 74 | .064 |
| 72 | .065 |
| 70 | .063 |
| 68 | .059 |
| 66 | .053 |
| 64 | .046 |
| 62 | .038 |
| 60 | .030 |
| 58 | .022 |
| 56 | .016 |
| 54 | .011 |

TABLE A4. PHOTODETACHMENT AND PHOTODISSOCIATION CROSS SECTIONS FOR ECLIPSE-66.

| WAVELENGTH RANGE (NM) | | REACTION NUMBERS | | | | | | | | | |
|---|---|---|---|---|---|---|---|---|---|---|---|
| FROM | TO | 1 | 2 | 3 | 4 | 5 | 6 | 7 | 8 | 9 | 10 |
| 100.0 - | 102.6 | 5.200E-18 | 5.500E-18 | 1.000E-18 | 1.000E-18 | 4.000E-18 | 1.000E-18 | 1.400E-18 | 1.000E-18 | 1.000E-18 | 1.000E-18 |
| 102.6 - | 105.3 | 5.200E-18 | 5.500E-18 | 1.000E-18 | 1.000E-18 | 4.000E-18 | 1.000E-18 | 1.400E-18 | 1.000E-18 | 1.000E-18 | 1.000E-18 |
| 105.3 - | 108.1 | 5.200E-18 | 5.500E-18 | 1.000E-18 | 1.000E-18 | 4.000E-18 | 1.000E-18 | 1.400E-18 | 1.000E-18 | 1.000E-18 | 1.000E-18 |
| 108.1 - | 111.1 | 5.200E-18 | 5.500E-18 | 1.000E-18 | 1.000E-18 | 4.000E-18 | 1.000E-18 | 1.400E-18 | 1.000E-18 | 1.000E-18 | 1.000E-18 |
| 111.1 - | 114.3 | 5.200E-18 | 5.600E-18 | 1.000E-18 | 1.000E-18 | 4.000E-18 | 1.000E-18 | 1.400E-18 | 1.000E-18 | 1.000E-18 | 1.000E-18 |
| 114.3 - | 117.6 | 5.200E-18 | 5.600E-18 | 1.000E-18 | 1.000E-18 | 4.000E-18 | 1.000E-18 | 1.400E-18 | 1.000E-18 | 1.000E-18 | 1.000E-18 |
| 117.6 - | 121.2 | 5.200E-18 | 5.600E-18 | 1.000E-18 | 1.000E-18 | 4.000E-18 | 1.000E-18 | 1.400E-18 | 1.000E-18 | 1.000E-18 | 1.000E-18 |
| 121.2 - | 125.0 | 5.200E-18 | 5.700E-18 | 1.000E-18 | 1.000E-18 | 4.000E-18 | 1.000E-18 | 1.400E-18 | 1.000E-18 | 1.000E-18 | 1.000E-18 |
| 125.0 - | 129.0 | 5.200E-18 | 5.700E-18 | 1.000E-18 | 1.000E-18 | 4.000E-18 | 1.000E-18 | 1.400E-18 | 1.000E-18 | 1.000E-18 | 1.000E-18 |
| 129.0 - | 133.3 | 5.200E-18 | 5.800E-18 | 1.000E-18 | 1.000E-18 | 4.000E-18 | 1.000E-18 | 1.400E-18 | 1.000E-18 | 1.000E-18 | 1.000E-18 |
| 133.3 - | 137.9 | 5.300E-18 | 5.900E-18 | 1.000E-18 | 1.000E-18 | 4.000E-18 | 1.000E-18 | 1.400E-18 | 1.000E-18 | 1.000E-18 | 1.000E-18 |
| 137.9 - | 142.9 | 5.300E-18 | 6.000E-18 | 1.000E-18 | 1.000E-18 | 4.000E-18 | 1.000E-18 | 1.400E-18 | 1.000E-18 | 1.000E-18 | 1.000E-18 |
| 142.9 - | 148.1 | 5.300E-18 | 6.100E-18 | 1.000E-18 | 1.000E-18 | 4.000E-18 | 1.000E-18 | 1.400E-18 | 1.000E-18 | 1.000E-18 | 1.000E-18 |
| 148.1 - | 153.8 | 5.300E-18 | 6.300E-18 | 1.000E-18 | 1.000E-18 | 4.000E-18 | 1.000E-18 | 1.400E-18 | 1.000E-18 | 1.000E-18 | 1.000E-18 |
| 153.8 - | 160.0 | 5.400E-18 | 6.400E-18 | 1.000E-18 | 1.000E-18 | 4.000E-18 | 1.000E-18 | 1.400E-18 | 1.000E-18 | 1.000E-18 | 1.000E-18 |
| 160.0 - | 166.7 | 5.400E-18 | 6.500E-18 | 1.000E-18 | 1.000E-18 | 4.000E-18 | 1.000E-18 | 1.400E-18 | 1.000E-18 | 1.000E-18 | 1.000E-18 |
| 166.7 - | 173.9 | 5.400E-18 | 6.700E-18 | 1.000E-18 | 1.000E-18 | 4.000E-18 | 1.000E-18 | 1.400E-18 | 1.000E-18 | 1.000E-18 | 1.000E-18 |
| 173.9 - | 181.8 | 5.500E-18 | 6.900E-18 | 1.000E-18 | 1.000E-18 | 4.000E-18 | 1.000E-18 | 1.400E-18 | 1.000E-18 | 1.000E-18 | 1.000E-18 |
| 181.8 - | 190.5 | 5.500E-18 | 7.300E-18 | 1.000E-18 | 1.000E-18 | 4.000E-18 | 1.000E-18 | 1.400E-18 | 1.000E-18 | 1.000E-18 | 1.000E-18 |
| 190.5 - | 200.0 | 5.600E-18 | 7.500E-18 | 1.000E-18 | 1.000E-18 | 4.000E-18 | 1.000E-18 | 1.400E-18 | 1.000E-18 | 1.000E-18 | 1.000E-18 |
| 200.0 - | 210.5 | 5.700E-18 | 7.700E-18 | 1.000E-18 | 1.000E-18 | 4.000E-18 | 1.000E-18 | 1.400E-18 | 1.000E-18 | 1.000E-18 | 1.000E-18 |
| 210.5 - | 222.2 | 5.800E-18 | 7.600E-18 | 1.000E-18 | 1.000E-18 | 4.000E-18 | 1.000E-18 | 1.400E-18 | 1.000E-18 | 1.000E-18 | 1.000E-18 |
| 222.2 - | 235.3 | 5.800E-18 | 5.900E-18 | 1.000E-18 | 1.000E-18 | 4.000E-18 | 1.000E-18 | 1.400E-18 | 1.000E-18 | 1.000E-18 | 1.000E-18 |
| 235.3 - | 250.0 | 5.900E-18 | 6.000E-18 | 1.000E-18 | 1.000E-18 | 4.000E-18 | 1.000E-18 | 1.400E-18 | 1.000E-18 | 1.000E-18 | 1.000E-18 |
| 250.0 - | 266.7 | 6.000E-18 | 6.200E-18 | 1.000E-18 | 1.000E-18 | 4.000E-18 | 1.000E-18 | 1.400E-18 | 1.000E-18 | 1.000E-18 | 1.000E-18 |
| 266.7 - | 285.7 | 6.000E-18 | 6.500E-18 | 1.000E-18 | 8.000E-19 | 4.000E-18 | 1.000E-18 | 1.400E-18 | 1.000E-18 | 1.000E-18 | 1.000E-18 |
| 285.7 - | 307.7 | 6.100E-18 | 6.700E-18 | 1.000E-18 | 3.000E-19 | 4.000E-18 | 1.000E-18 | 1.400E-18 | 1.000E-18 | 1.000E-18 | 1.000E-18 |
| 307.7 - | 333.3 | 6.200E-18 | 6.600E-18 | 1.000E-18 | 1.000E-19 | 4.000E-18 | 1.000E-18 | 1.400E-18 | 1.000E-18 | 1.000E-18 | 1.000E-18 |
| 333.3 - | 363.6 | 6.200E-18 | 4.800E-18 | 1.000E-18 | 1.000E-20 | 3.500E-18 | 1.000E-18 | 1.400E-18 | 1.000E-18 | 1.000E-18 | 1.000E-18 |
| 363.6 - | 400.0 | 6.300E-18 | 0. | 1.000E-18 | 0. | 2.900E-18 | 9.000E-19 | 1.400E-18 | 1.000E-18 | 1.000E-18 | 1.000E-18 |
| 400.0 - | 430.0 | 6.300E-18 | 0. | 1.000E-18 | 0. | 2.400E-18 | 9.000E-19 | 1.400E-18 | 1.000E-18 | 1.000E-18 | 1.000E-18 |
| 430.0 - | 470.0 | 6.300E-18 | 0. | 9.000E-19 | 0. | 2.200E-18 | 9.000E-19 | 1.200E-18 | 1.000E-18 | 1.000E-18 | 1.000E-18 |
| 470.0 - | 510.0 | 6.300E-18 | 0. | 4.000E-19 | 0. | 1.800E-18 | 8.000E-19 | 7.000E-19 | 1.000E-18 | 1.000E-18 | 1.000E-18 |
| 510.0 - | 560.0 | 6.300E-18 | 0. | 1.000E-19 | 0. | 1.500E-18 | 3.000E-19 | 1.300E-18 | 1.000E-18 | 1.000E-18 | 1.000E-18 |
| 560.0 - | 620.0 | 6.200E-18 | 0. | 5.000E-20 | 0. | 1.300E-18 | 3.000E-20 | 1.400E-18 | 1.000E-18 | 1.000E-18 | 1.000E-18 |
| 620.0 - | 680.0 | 5.800E-18 | 0. | 0. | 0. | 1.100E-18 | 0. | 0. | 1.000E-18 | 1.000E-18 | 1.000E-18 |
| 680.0 - | 730.0 | 5.400E-18 | 0. | 0. | 0. | 9.000E-19 | 0. | 0. | 1.000E-18 | 1.000E-18 | 1.000E-18 |

PHOTODISSOCIATION CROSSECTIONS (CM**2) USED IN SUBPROGRAM BLKDAT - 75/12/16

| WAVELENGTH RANGE (NM) | | REACTION NUMBERS | | | | | | | | | |
|---|---|---|---|---|---|---|---|---|---|---|---|
| FROM | TO | 11 | 12 | 13 | 14 | 15 | 16 | 17 | 18 | 19 | 20 |
| 100.0 - | 102.6 | 1.000E-18 | 1.000E-18 | 1.000E-18 | 1.000E-18 | 1.000E-18 | 4.400E-17 | 1.000E-18 | 1.040E-17 | 1.000E-18 | 0. |
| 102.6 - | 105.3 | 1.000E-18 | 1.000E-18 | 1.000E-18 | 1.000E-18 | 1.000E-18 | 1.800E-17 | 1.000E-18 | 5.100E-18 | 1.000E-18 | 0. |
| 105.3 - | 108.1 | 1.000E-18 | 1.000E-18 | 1.000E-18 | 1.000E-18 | 1.000E-18 | 1.000E-17 | 1.000E-18 | 3.100E-18 | 1.000E-18 | 0. |
| 108.1 - | 111.1 | 1.000E-18 | 1.000E-18 | 1.000E-18 | 1.000E-18 | 1.000E-18 | 1.100E-17 | 1.000E-18 | 1.200E-18 | 9.000E-18 | 0. |
| 111.1 - | 114.3 | 1.000E-18 | 1.000E-18 | 1.000E-18 | 1.000E-18 | 1.000E-18 | 5.000E-17 | 1.000E-18 | 7.000E-19 | 8.200E-18 | 0. |
| 114.3 - | 117.6 | 1.000E-18 | 1.000E-18 | 1.000E-18 | 1.000E-18 | 1.000E-18 | 1.500E-18 | 1.000E-18 | 4.000E-19 | 7.000E-18 | 0. |
| 117.6 - | 121.2 | 1.000E-18 | 1.000E-18 | 1.000E-18 | 1.000E-18 | 1.000E-18 | 4.000E-20 | 1.000E-18 | 3.000E-19 | 7.300E-18 | 0. |
| 121.2 - | 125.0 | 1.000E-18 | 1.000E-18 | 1.000E-18 | 1.000E-18 | 1.000E-18 | 1.300E-19 | 1.000E-18 | 4.000E-19 | 1.100E-17 | 0. |
| 125.0 - | 129.0 | 1.000E-18 | 1.000E-18 | 1.000E-18 | 1.000E-18 | 1.000E-18 | 4.000E-19 | 1.000E-18 | 1.100E-18 | 1.500E-17 | 0. |
| 129.0 - | 133.3 | 1.000E-18 | 1.000E-18 | 1.000E-18 | 1.000E-18 | 1.000E-18 | 8.000E-19 | 1.000E-18 | 1.900E-18 | 1.100E-17 | 0. |
| 133.3 - | 137.9 | 1.000E-18 | 1.000E-18 | 1.000E-18 | 1.000E-18 | 1.000E-18 | 9.000E-19 | 1.000E-18 | 2.000E-18 | 9.300E-18 | 0. |
| 137.9 - | 142.9 | 1.000E-18 | 1.000E-18 | 1.000E-18 | 1.000E-18 | 1.000E-18 | 8.000E-19 | 1.000E-18 | 2.500E-18 | 1.300E-17 | 0. |
| 142.9 - | 148.1 | 1.000E-18 | 1.000E-18 | 1.000E-18 | 1.000E-18 | 1.000E-18 | 9.000E-19 | 1.000E-18 | 2.500E-18 | 1.300E-17 | 0. |
| 148.1 - | 153.8 | 1.000E-18 | 1.000E-18 | 1.000E-18 | 1.000E-18 | 1.000E-18 | 7.000E-19 | 1.000E-18 | 1.200E-18 | 1.300E-17 | 0. |
| 153.8 - | 160.0 | 1.000E-18 | 1.000E-18 | 1.000E-18 | 1.000E-18 | 1.000E-18 | 4.000E-19 | 1.000E-18 | 3.000E-19 | 1.500E-17 | 0. |
| 160.0 - | 166.7 | 1.000E-18 | 1.000E-18 | 1.000E-18 | 1.000E-18 | 1.000E-18 | 1.500E-19 | 1.000E-18 | 2.000E-19 | 1.500E-17 | 0. |
| 166.7 - | 173.9 | 1.000E-18 | 1.000E-18 | 1.000E-18 | 1.000E-18 | 1.000E-18 | 1.000E-20 | 1.000E-18 | 1.500E-19 | 1.500E-17 | 0. |
| 173.9 - | 181.8 | 1.000E-18 | 1.000E-18 | 1.000E-18 | 1.000E-18 | 1.000E-18 | 1.000E-21 | 1.000E-18 | 2.000E-19 | 1.000E-17 | 3.000E-22 |
| 181.8 - | 190.5 | 1.000E-18 | 1.000E-18 | 1.000E-18 | 1.000E-18 | 1.000E-18 | 1.000E-22 | 1.000E-18 | 1.500E-19 | 2.200E-18 | 1.200E-23 |
| 190.5 - | 200.0 | 1.000E-18 | 1.000E-18 | 1.000E-18 | 1.000E-18 | 1.000E-18 | 5.000E-24 | 9.100E-18 | 0. | 4.200E-19 | 1.200E-23 |
| 200.0 - | 210.5 | 1.000E-18 | 1.000E-18 | 1.000E-18 | 1.000E-18 | 1.000E-18 | 3.000E-24 | 2.500E-18 | 0. | 4.000E-19 | 9.000E-24 |
| 210.5 - | 222.2 | 1.000E-18 | 1.000E-18 | 1.000E-18 | 1.000E-18 | 1.000E-18 | 2.000E-24 | 2.500E-19 | 0. | 4.500E-19 | 1.000E-23 |
| 222.2 - | 235.3 | 1.000E-18 | 1.000E-18 | 1.000E-18 | 1.000E-18 | 1.000E-18 | 0. | 7.000E-20 | 0. | 2.500E-19 | 5.000E-24 |
| 235.3 - | 250.0 | 1.000E-18 | 1.000E-18 | 1.000E-18 | 1.000E-18 | 1.000E-18 | 0. | 2.400E-20 | 0. | 5.400E-20 | 1.000E-24 |
| 250.0 - | 266.7 | 1.000E-18 | 1.000E-18 | 1.000E-18 | 1.000E-18 | 1.000E-18 | 0. | 1.900E-20 | 0. | 1.900E-20 | 0. |
| 266.7 - | 285.7 | 1.000E-18 | 1.000E-18 | 1.000E-18 | 1.000E-18 | 1.000E-18 | 0. | 1.400E-20 | 0. | 5.100E-20 | 0. |
| 285.7 - | 307.7 | 1.000E-18 | 1.000E-18 | 1.000E-18 | 1.000E-18 | 1.000E-18 | 0. | 4.000E-21 | 0. | 1.200E-19 | 0. |
| 307.7 - | 333.3 | 1.000E-18 | 1.000E-18 | 1.000E-18 | 1.000E-18 | 1.000E-18 | 0. | 2.000E-22 | 0. | 3.000E-19 | 0. |
| 333.3 - | 363.6 | 1.000E-18 | 1.000E-18 | 1.000E-18 | 1.000E-18 | 1.000E-18 | 0. | 0. | 0. | 5.100E-19 | 0. |
| 363.6 - | 400.0 | 1.000E-18 | 1.000E-18 | 1.000E-18 | 1.000E-18 | 1.000E-18 | 0. | 0. | 0. | 6.300E-19 | 0. |
| 400.0 - | 430.0 | 1.000E-18 | 1.000E-18 | 1.000E-18 | 1.000E-18 | 1.000E-18 | 0. | 0. | 0. | 6.000E-20 | 0. |
| 430.0 - | 470.0 | 1.000E-18 | 1.000E-18 | 1.000E-18 | 1.000E-18 | 1.000E-18 | 0. | 0. | 0. | 0. | 0. |
| 470.0 - | 510.0 | 1.000E-18 | 1.000E-18 | 1.000E-18 | 1.000E-18 | 1.000E-18 | 0. | 0. | 0. | 0. | 0. |
| 510.0 - | 560.0 | 1.000E-18 | 0. | 1.000E-18 | 1.000E-18 | 1.000E-18 | 0. | 0. | 0. | 0. | 0. |
| 560.0 - | 620.0 | 1.000E-18 | 0. | 1.000E-18 | 1.000E-18 | 1.000E-18 | 0. | 0. | 0. | 0. | 0. |
| 620.0 - | 680.0 | 1.000E-18 | 0. | 1.000E-18 | 1.000E-18 | 1.000E-18 | 0. | 0. | 0. | 0. | 0. |
| 680.0 - | 730.0 | 1.000E-18 | 0. | 1.000E-18 | 1.000E-18 | 1.000E-18 | 0. | 0. | 0. | 0. | 0. |

PHOTODISSOCIATION CROSSECTIONS (CM**2) USED IN SUBPROGRAM RLKDAT - 75/12/16

| WAVELENGTH RANGE (NM) | | REACTION NUMBERS | | | | | | | | | |
|---|---|---|---|---|---|---|---|---|---|---|---|
| FROM | TO | 21 | 22 | 23 | 24 | 25 | 26 | 27 | 28 | 29 | 30 |
| 100.0 - | 102.6 | 4.000E-19 | 0. | 0. | 1.000E-18 | 0. | 1.000E-20 | 0. | 1.000E-18 | 1.000E-18 | 8.000E-18 |
| 102.6 - | 105.3 | 1.000E-18 | 0. | 0. | 1.000E-18 | 0. | 1.000E-20 | 0. | 1.000E-18 | 1.000E-18 | 4.000E-18 |
| 105.3 - | 108.1 | 5.000E-20 | 0. | 0. | 9.300E-18 | 0. | 1.000E-20 | 0. | 1.000E-18 | 1.000E-18 | 6.000E-18 |
| 108.1 - | 111.1 | 4.300E-21 | 0. | 0. | 9.300E-18 | 0. | 1.000E-20 | 0. | 1.000E-18 | 1.000E-18 | 5.000E-18 |
| 111.1 - | 114.3 | 1.000E-20 | 0. | 0. | 1.040E-17 | 0. | 1.000E-20 | 0. | 1.000E-18 | 0. | 1.000E-18 |
| 114.3 - | 117.6 | 1.000E-20 | 0. | 0. | 6.700E-18 | 0. | 1.000E-20 | 0. | 1.000E-18 | 0. | 1.000E-18 |
| 117.6 - | 121.2 | 7.000E-21 | 0. | 0. | 9.300E-18 | 0. | 1.000E-20 | 0. | 1.000E-18 | 0. | 1.000E-18 |
| 121.2 - | 125.0 | 1.000E-20 | 0. | 0. | 1.500E-17 | 0. | 1.000E-20 | 0. | 1.000E-18 | 0. | 6.000E-18 |
| 125.0 - | 129.0 | 6.500E-20 | 0. | 0. | 7.100E-18 | 0. | 1.000E-20 | 0. | 1.000E-18 | 0. | 7.000E-18 |
| 129.0 - | 133.3 | 1.000E-18 | 0. | 0. | 1.300E-17 | 0. | 1.000E-20 | 0. | 1.000E-18 | 0. | 6.000E-18 |
| 133.3 - | 137.9 | 6.000E-18 | 0. | 0. | 9.300E-18 | 0. | 1.000E-20 | 0. | 1.000E-18 | 0. | 3.000E-18 |
| 137.9 - | 142.9 | 1.400E-17 | 0. | 0. | 7.400E-18 | 0. | 1.000E-20 | 0. | 1.000E-18 | 0. | 7.000E-19 |
| 142.9 - | 148.1 | 1.400E-17 | 0. | 0. | 5.600E-18 | 0. | 1.000E-20 | 0. | 1.000E-18 | 0. | 6.000E-19 |
| 148.1 - | 153.8 | 1.200E-17 | 0. | 0. | 3.300E-18 | 0. | 1.000E-20 | 0. | 1.000E-18 | 0. | 1.200E-18 |
| 153.8 - | 160.0 | 8.000E-18 | 0. | 0. | 1.120E-18 | 0. | 1.000E-20 | 0. | 1.000E-18 | 0. | 2.000E-18 |
| 160.0 - | 166.7 | 3.500E-18 | 0. | 0. | 9.300E-19 | 0. | 1.000E-20 | 0. | 1.000E-18 | 0. | 4.500E-18 |
| 166.7 - | 173.9 | 3.000E-19 | 0. | 0. | 8.200E-19 | 0. | 1.000E-20 | 0. | 1.000E-18 | 0. | 3.200E-18 |
| 173.9 - | 181.8 | 3.000E-22 | 0. | 0. | 7.400E-19 | 0. | 1.000E-20 | 0. | 1.000E-18 | 0. | 3.000E-19 |
| 181.8 - | 190.5 | 1.200E-23 | 0. | 0. | 6.700E-19 | 0. | 1.000E-20 | 0. | 3.800E-18 | 0. | 5.000E-21 |
| 190.5 - | 200.0 | 1.200E-23 | 0. | 0. | 4.100E-19 | 0. | 1.000E-20 | 0. | 4.300E-18 | 0. | 6.000E-23 |
| 200.0 - | 210.5 | 9.000E-24 | 0. | 0. | 3.300E-19 | 0. | 1.000E-20 | 0. | 4.600E-18 | 0. | 0. |
| 210.5 - | 222.2 | 1.000E-23 | 0. | 0. | 1.100E-18 | 0. | 1.000E-20 | 0. | 4.200E-18 | 0. | 0. |
| 222.2 - | 235.3 | 5.000E-24 | 0. | 0. | 4.000E-18 | 0. | 1.000E-20 | 0. | 2.900E-18 | 0. | 0. |
| 235.3 - | 250.0 | 1.000E-24 | 0. | 0. | 9.200E-18 | 0. | 1.000E-20 | 0. | 1.100E-18 | 0. | 0. |
| 250.0 - | 266.7 | 0. | 0. | 0. | 1.100E-17 | 0. | 1.000E-20 | 0. | 4.000E-19 | 0. | 0. |
| 266.7 - | 285.7 | 0. | 0. | 0. | 5.600E-18 | 0. | 1.000E-20 | 0. | 1.000E-19 | 0. | 0. |
| 285.7 - | 307.7 | 0. | 0. | 0. | 6.000E-19 | 0. | 8.300E-21 | 0. | 0. | 0. | 0. |
| 307.7 - | 333.3 | 0. | 0. | 2.000E-20 | 0. | 0. | 1.900E-20 | 0. | 0. | 0. | 0. |
| 333.3 - | 363.6 | 0. | 0. | 5.000E-22 | 0. | 0. | 4.200E-20 | 0. | 0. | 0. | 0. |
| 363.6 - | 400.0 | 0. | 0. | 0. | 0. | 0. | 3.100E-20 | 0. | 0. | 0. | 0. |
| 400.0 - | 430.0 | 0. | 4.140E-23 | 0. | 0. | 0. | 0. | 0. | 0. | 0. | 0. |
| 430.0 - | 470.0 | 0. | 1.920E-22 | 0. | 0. | 0. | 0. | 0. | 0. | 0. | 0. |
| 470.0 - | 510.0 | 0. | 8.780E-22 | 0. | 0. | 0. | 0. | 0. | 0. | 0. | 0. |
| 510.0 - | 560.0 | 0. | 2.480E-21 | 0. | 0. | 0. | 0. | 0. | 0. | 0. | 0. |
| 560.0 - | 620.0 | 0. | 4.250E-21 | 0. | 0. | 0. | 0. | 0. | 0. | 0. | 0. |
| 620.0 - | 680.0 | 0. | 2.650E-21 | 0. | 0. | 0. | 0. | 0. | 0. | 0. | 0. |
| 680.0 - | 730.0 | 0. | 8.900E-22 | 0. | 0. | 0. | 0. | 0. | 0. | 0. | 0. |

PHOTODISSOCIATION CROSSECTIONS (CM+2) USED IN SUBPROGRAM BLKDAT - 75/12/16

| WAVELENGTH RANGE (NM) | | REACTION NUMBERS | | | | | | |
|---|---|---|---|---|---|---|---|---|
| FROM | TO | 31 | 32 | 33 | 34 | 35 | 36 | 37 |
| 100.0 - | 102.6 | 0. | 1.000E-18 | 0. | 0. | 1.000E-18 | 0. | 5.200E-18 |
| 102.6 - | 105.3 | 0. | 1.000E-18 | 0. | 0. | 1.000E-18 | 0. | 5.200E-18 |
| 105.3 - | 108.1 | 0. | 1.000E-18 | 0. | 0. | 1.000E-18 | 0. | 5.200E-18 |
| 108.1 - | 111.1 | 0. | 1.000E-18 | 0. | 0. | 3.700E-17 | 0. | 5.200E-18 |
| 111.1 - | 114.3 | 0. | 1.000E-18 | 0. | 0. | 2.600E-17 | 0. | 5.200E-18 |
| 114.3 - | 117.6 | 0. | 1.000E-18 | 0. | 0. | 1.100E-17 | 0. | 5.200E-18 |
| 117.6 - | 121.2 | 0. | 1.000E-18 | 0. | 0. | 3.700E-18 | 0. | 5.200E-18 |
| 121.2 - | 125.0 | 0. | 1.000E-18 | 0. | 0. | 5.600E-18 | 0. | 5.200E-18 |
| 125.0 - | 129.0 | 0. | 1.000E-18 | 0. | 0. | 7.100E-17 | 0. | 5.200E-18 |
| 129.0 - | 133.3 | 0. | 1.000E-18 | 0. | 0. | 5.600E-17 | 0. | 5.300E-18 |
| 133.3 - | 137.9 | 0. | 1.000E-18 | 0. | 0. | 2.600E-18 | 0. | 5.300E-18 |
| 137.9 - | 142.9 | 0. | 1.000E-18 | 0. | 0. | 1.700E-18 | 0. | 5.300E-18 |
| 142.9 - | 148.1 | 0. | 1.000E-18 | 0. | 0. | 6.300E-18 | 0. | 5.300E-18 |
| 148.1 - | 153.8 | 0. | 1.000E-18 | 0. | 0. | 9.300E-19 | 0. | 5.400E-18 |
| 153.8 - | 160.0 | 0. | 1.000E-18 | 0. | 0. | 7.800E-20 | 0. | 5.400E-18 |
| 160.0 - | 166.7 | 0. | 1.000E-18 | 0. | 0. | 4.800E-20 | 0. | 5.400E-18 |
| 166.7 - | 173.9 | 0. | 1.000E-18 | 0. | 0. | 8.900E-20 | 0. | 5.500E-18 |
| 173.9 - | 181.8 | 0. | 1.000E-18 | 0. | 0. | 1.400E-19 | 0. | 5.500E-18 |
| 181.8 - | 190.5 | 0. | 1.000E-18 | 0. | 0. | 1.300E-19 | 0. | 5.600E-18 |
| 190.5 - | 200.0 | 0. | 6.000E-19 | 0. | 0. | 8.000E-20 | 0. | 5.700E-18 |
| 200.0 - | 210.5 | 0. | 4.600E-19 | 0. | 0. | 1.500E-20 | 0. | 5.800E-18 |
| 210.5 - | 222.2 | 0. | 3.300E-19 | 0. | 0. | 1.500E-21 | 0. | 5.800E-18 |
| 222.2 - | 235.3 | 0. | 2.200E-19 | 0. | 0. | 1.000E-22 | 0. | 5.900E-18 |
| 235.3 - | 250.0 | 0. | 1.200E-19 | 0. | 0. | 1.300E-23 | 0. | 6.000E-18 |
| 250.0 - | 266.7 | 0. | 7.000E-20 | 0. | 0. | 5.000E-24 | 0. | 6.000E-18 |
| 266.7 - | 285.7 | 0. | 3.000E-20 | 0. | 0. | 6.000E-24 | 0. | 6.100E-18 |
| 285.7 - | 307.7 | 0. | 1.200E-20 | 0. | 0. | 4.000E-24 | 0. | 6.200E-18 |
| 307.7 - | 333.3 | 0. | 5.000E-21 | 0. | 0. | 1.000E-24 | 0. | 6.200E-18 |
| 333.3 - | 363.6 | 0. | 2.000E-21 | 0. | 0. | 0. | 0. | 6.300E-18 |
| 363.6 - | 400.0 | 0. | 3.000E-22 | 0. | 0. | 0. | 0. | 6.300E-18 |
| 400.0 - | 430.0 | 0. | 0. | 0. | 0. | 0. | 0. | 6.300E-18 |
| 430.0 - | 470.0 | 0. | 0. | 0. | 0. | 0. | 0. | 6.300E-18 |
| 470.0 - | 510.0 | 0. | 0. | 0. | 0. | 0. | 0. | 6.300E-18 |
| 510.0 - | 560.0 | 0. | 0. | 0. | 0. | 0. | 0. | 6.200E-18 |
| 560.0 - | 620.0 | 0. | 0. | 0. | 0. | 0. | 0. | 5.800E-18 |
| 620.0 - | 680.0 | 0. | 0. | 0. | 0. | 0. | 0. | 5.400E-18 |
| 680.0 - | 730.0 | 0. | 0. | 0. | 0. | 0. | 0. | 0. |

TABLE A5. PHOTOLYTIC REACTIONS AND REFERENCES FOR ECLIPSE-66.

| REAC. NO. | REACTION | WAVELENGTH REGION | REFERENCE | REF. NO. |
|---|---|---|---|---|
| 1 | O- + HV = O + E | 100-116 NM, BANDS 11-16 | EXTRAPOLATION FROM CHURCHILL, SEE TEXT | 1 |
| | | 116-730 NM, BANDS 16-47 | CHURCHILL ET AL, JQSRT V6, P371-442 1966 | 1 |
| 2 | O- + HV = O1D + E | 100-116 NM, BANDS 11-16 | EXTRAPOLATION FROM CHURCHILL, SEE TEXT | 2 |
| | | 116-730 NM, BANDS 16-47 | CHURCHILL ET AL, JQSRT V6, P371-442 1966 | 2 |
| 3 | NO2- + HV = NO2 + E | 100-430 NM, BANDS 11-41 | ESTIMATED, SEE TEXT | 3 |
| | | 430-560 NM, BANDS 42-44 | HERBST ET AL, JCP V61 P1300-4 FIG 3, 1974 | 3 |
| | | | BUT SEE TEXT | 3 |
| 4 | NO3- + HV = O + NO2 + E | 100-267 NM, BANDS 11-35 | ESTIMATED, SEE TEXT | 4 |
| | | 267-364 NM, BANDS 36-39 | ESTIMATED, SEE TEXT, USED NO2- SHAPE SHIFTED | 4 |
| 5 | O2- + HV = O2 + E | 100-450 NM, BANDS 11-41 | ESTIMATED, SEE TEXT | 5 |
| | | 440-730 NM, BANDS 42-47 | BURCH ET AL, PHYS REV V112 P 171 1958 | 5 |
| | | 440-730 NM, BANDS 42-47 | BURCH ET AL, PHYS REV V114 P 1652, 1959 | 5 |
| 6 | O3- + HV = O3 + E | 100-450 NM, BANDS 11-42 | ESTIMATED, SEE TEXT | 6 |
| | | 440-730 NM, BANDS 43-46 | COSBY ET AL JCP V63 P1612-20 1975 | 6 |
| 7 | CO3- + HV = CO2 + O- | 100-450 NM, BANDS 11-42 | ESTIMATED, SEE TEXT | 7 |
| | | 430-510 NM, BANDS 42-43 | MOSELEY ET AL, CHEM PHYS LET V26 P288-91 1974 | 7 |
| | | 510-740 NM, BANDS 44-47 | ESTIMATED, SEE TEXT | 7 |
| 8 | 78- + HV = CO3- + H2O | 100-470 NM, BANDS 11-42 | ESTIMATED, SEE TEXT | 8 |
| | | 470-510 NM, BAND 43 | MOSELEY ET AL CHEM P LET V26 P288-91 1974 | 8 |
| | | 510-740 NM, BANDS 44-47 | ESTIMATED, SEE TEXT | 8 |
| 9 | CO4- + HV = O2- + CO2 | 100-740 NM, BANDS 11-47 | ESTIMATED, SEE TEXT | 9 |
| | | 510-680 NM, BANDS 44-46 | J MOSFLEY, JCP V65 N12 P5267-74 1976 | 9 |
| | | 680-740 NM, BAND 47 | ESTIMATED, SEE TEXT | 9 |
| 10 | 94- + HV = CO4- + H2O | 100-740 NM, BANDS 11-47 | ESTIMATED, SEE TEXT | 10 |
| 11 | 64- + HV = NO2- + H2O | 100-740 NM, BANDS 11-47 | ESTIMATED, SEE TEXT | 11 |
| 12 | 62- + HV = NO + O2- | 100-740 NM, BANDS 11-47 | ESTIMATED, SEE TEXT, NO3- ISOMER | 12 |
| 13 | 80- + HV = NO3- + H2O | 100-740 NM, BANDS 11-47 | ESTIMATED, SEE TEXT | 13 |
| 14 | O2-W + HV = O2- + H2O | 100-740 NM, BANDS 11-47 | ESTIMATED, SEE TEXT | 14 |
| 15 | O4- + HV = O2- + O2 | 100-740 NM, BANDS 11-47 | ESTIMATED, SEE TEXT | 15 |
| 16 | CO2 + HV = CO + O | 100-111 NM, BANDS 11-14 | LAWRENCE JCP V 56 P3435-42 1972 | 16 |
| | | 105-125 NM, BANDS 13-18 | INN AT AL JCP V21 P1648-50 1953 | 16 |
| | | 121-200 NM, BANDS 18-30 | DNA 1948H RRH P12-16 F 12-16 1972 | 16 |
| | | 174-222 NM, BANDS 28-32 | ACKERMAN ANN GEOPHYS V28 P79-63 1972 | 16 |
| 17 | HNO3 + HV = HO + NO2 | 100-125 NM,BANDS 11-18 | ESTIMATED, SEE TEXT | 17 |
| | | 125-167 NM,BANDS 19-26 | JOHNSTON + GRAHAM CAN J CHEM V52 P1415-22 1974 | 17 |
| 18 | NO + HV = N + O | 100-191 NM, BANDS 11-29 | DNA 1948H RRH REV 1972 | 18 |
| 19 | NO2 + HV = NO + O | 100-108 NM,BANDS 11-13 | ESTIMATED, SEE TEXT | 19 |
| | | 190-286 NM,BANDS 30-36 | JOHNSTON + GRAHAM CAN J CHEM V52 P1415-23 1974 | 19 |
| 20 | O2 + HV = O + O | 286-400 NM,BANDS 37-40 | NBSIR 73-207 GARVIN ED 1973 | 19 |
| | | | SEE TEXT FOR SQUARE ROOT LAW | 20 |
| 21 | O2 + HV = O + O1D | 174-250 NM,BANDS 28-34 | ACKERMAN ET AL PLNT + SPA SCI V18 P1639-51 1970 | 20 |
| | | | SEE TEXT FOR SQUARE ROOT LAW | 21 |
| 22 | O3 + HV = O + O2 | 100-111 NM, BANDS 11-14 | D M HUNTEN + M B MCELROY JGR V73 P2421-8 1968 | 21 |
| 23 | O3 + HV = O + O2 | 111-129 NM, BANDS 14-19 | R D HUDSON RGP+SP V9 P305-406 1971 | 21 |
| 24 | O3 + HV = O1D + O2 | 125-174 NM BANDS 19-27 | BLAKE ET AL JQSRT V6 PP451-9 FIG5 1966 | 21 |
| | | 400-730 NM, BANDS 41-47 | JOHNSTON + GRAHAM CAN J CH V52 P1415-23 1974 | 22 |
| 25 | HNO2 + HV = H + NO2 | 308-364 NM, BANDS 38-39 | R D HUDSON RGP+SP V9 P305-406 1971 | 23 |
| 26 | HNO2 + HV = HO + NO | 100-105 NM, BANDS 11-12 | ESTIMATED, SEE TEXT | 24 |
| | | 105-222 NM, BANDS 13-32 | Y TANAKA ET AL J C P V21 P1651-53 1953 | 24 |
| 27 | HO2 + HV = H + O2 | 200-308 NM, BANDS 31-37 | R D HUDSON RGP+SP V9 P305-406 1971 | 24 |
| 28 | HO2 + HV = HO + O | | NOT COMPUTED | 25 |
| | | 100-286 NM,BANDS 11-36 | ESTIMATED, SEE TEXT | 26 |
| 29 | H2 + HV = H + H | 286-400 NM,BANDS 37-40 | JOHNSTON + GRAHAM CAN J CHEM V52 P1415-23 1974 | 26 |
| 30 | H2O + HV = H + HO | | NOT COMPUTED | 27 |
| | | 100-125 NM,BANDS 11-18 | ESTIMATED, SEE TEXT | 28 |
| | | 125-167 NM,BANDS 19-26 | J TROE IN NBSIR-73-206, GARVIN ED, 1973 | 28 |
| | | 100-111 NM, BANDS 11-14 | ESTIMATED, SEE TEXT | 29 |
| | | 100-111 NM, BANDS 11-14 | R D HUDSON, RGP+SP V9 P305-406 1971 | 30 |
| | | 111-121 NM,BANDS 15-17 | ESTIMATED, SEE TEXT | 30 |
| | | 121-190 NM, BANDS 18-24 | R D HUDSON + DNA 1964H RRH REV 1972 | 30 |

| REAC. NO. | REACTION | WAVELENGTH REGION | REFERENCE | REF. NO. |
|---|---|---|---|---|
| 31 | $H_2O_2 + HV = H_2O + O$ | 190-200 NM, BAND 30 | THOMPSON ET AL, ADV PHOTOCHEM V3, P192 | 30 |
| 32 | $H_2O_2 + HV = HO + HO$ | | NOT COMPUTED | 31 |
| | | 100-125 NM, BANDS 11-18 | ESTIMATED, SEE TEXT | 32 |
| | | 125-142 NM, BANDS 19-22 | HAMPSON JPCRD V2 P290-291 1973 | 32 |
| 33 | $N_2O + HV = N + NO$ | 138-200 NM, BANDS 22-30 | UREY ET AL JACS V51 P1371-83 1929 | 32 |
| 34 | $N_2O + HV = N_2 + O$ | | NOT COMPUTED | 33 |
| 35 | $N_2O + HV = N_2 + O1D$ | | NOT COMPUTED | 34 |
| | | 100-108 NM, BANDS 11-13 | ESTIMATED, SEE TEXT | 35 |
| | | 108-182 NM, BANDS 14-26 | ZELIKOFF ET AL JCP V21 P1643-7 1953 | 35 |
| 36 | $OH + HV = O + H$ | 182-333 NM, BANDS 29-38 | JOHNSTON + GRAHAM CAN J CHEM V52 P1415-23 1974 | 35 |
| 37 | $N + HV = N+ + E$ | | NOT COMPUTED | 36 |
| | | 0.4-10 NM, BANDS 1-10 | W SWIDER RGP+SP V7 P573-94, 1969 | 37 |
| | | GAMMA- X-RAY PRE ELECT | SEE IONIZATION SECTION OF TEXT | 37 |
| 38 | $N_2 + HV = N_2+ + E$ | 0.4-10 NM, BANDS 1-10 | W SWIDER RGP+SP V7 P573-94, 1969 | 38 |
| | | GAMMA- X-RAY PRE ELECT | SEE IONIZATION SECTION OF TEXT | 38 |
| 39 | $NO + HV = NO+ + E$ | 0.4-10 NM, BANDS 1-10 | W SWIDER RGP+SP V7 P573-94, 1969 | 39 |
| | | GAMMA- X-RAY PRE ELECT | SEE IONIZATION SECTION OF TEXT | 39 |
| | | 100-114 NM, BANDS 11-15 | WATANABE ET AL APLD OPT V6 P391-6, P1220 1967 | 39 |
| | | 114-135 NM, BANDS 16-20 | DNA 1948H RRH 1972 | 39 |
| 40 | $NO2 + HV = NO2+ + E$ | 0.4-10 NM, BANDS 1-10 | W SWIDER RGP+SP V7 P573-94, 1969 | 40 |
| | | GAMMA- X-RAY PRE ELECT | SEE IONIZATION SECTION OF TEXT | 40 |
| | | 100-114 NM, BANDS 11-14 | ESTIMATED | 40 |
| | | 114-129 NM, BANDS 15-19 | NAKAYAMA ET AL JCP V30 P1180-6 1959 | 40 |
| 41 | $O + HV = O+ + E$ | 0.4-10 NM, BANDS 1-10 | W SWIDER RGP+SP V7 P573-94, 1969 | 41 |
| | | GAMMA- X-RAY PRE ELECT | SEE IONIZATION SECTION OF TEXT | 41 |
| 42 | $O2 + HV = O2+ + E$ | 0.4-10 NM, BANDS 1-10 | W SWIDER RGP+SP V7 P573-94, 1969 | 42 |
| | | GAMMA- X-RAY PRE ELECT | SEE IONIZATION SECTION OF TEXT | 42 |
| | | 100-103 NM, BAND 11 | DNA 1948H RRH 1972 | 42 |
| 43 | $O21D + HV = O2+ + E$ | 0.4-10 NM, BANDS 1-10 | W SWIDER RGP+SP V7 P573-94, 1969 | 43 |
| | | GAMMA- X-RAY PRE ELECT | SEE IONIZATION SECTION OF TEXT | 43 |
| | | 100-105 NM, BANDS 11-12 | ESTIMATED | 43 |
| | | 105-112 NM, BANDS 13-15 | R P WAYNE IN MMRE G FIOCCO ED P 240-52 1971 | 43 |
| 44 | $N2 + HV = N + N+ + E$ | 0.4-10 NM, BANDS 1-10 | W SWIDER RGP+SP V7 P573-94, 1969 | 44 |
| | | GAMMA- X-RAY PRE ELECT | SEE IONIZATION SECTION OF TEXT | 44 |
| 45 | $O2 + HV = O + O+ + E$ | 0.4-10 NM, BANDS 1-10 | W SWIDER RGP+SP V7 P573-94, 1969 | 45 |
| | | GAMMA- X-RAY PRE ELECT | SEE IONIZATION SECTION OF TEXT | 45 |

TABLE A6. ULTRAVIOLET AND X-RAY ECLIPSE FUNCTIONS FOR ECLIPSE-66

| TIME | UV | $X_{in}$ | $X_{out}$ |
|---|---|---|---|
| 0 | .000 | .170 | .165 |
| 100 | .008 | .175 | .165 |
| 200 | .018 | .180 | .170 |
| 300 | .033 | .190 | .170 |
| 400 | .044 | .200 | .175 |
| 500 | .068 | .210 | .185 |
| 600 | .089 | .225 | .190 |
| 700 | .112 | .240 | .200 |
| 800 | .136 | .255 | .215 |
| 900 | .161 | .270 | .225 |
| 1000 | .188 | .290 | .240 |
| 1100 | .215 | .315 | .250 |
| 1200 | .243 | .340 | .265 |
| 1300 | .272 | .370 | .285 |
| 1400 | .302 | .405 | .300 |
| 1500 | .331 | .455 | .320 |
| 1600 | .360 | .505 | .340 |
| 1700 | .390 | .545 | .365 |
| 1800 | .420 | .575 | .380 |
| 1900 | .449 | .600 | .395 |
| 2000 | .479 | .630 | .410 |
| 2100 | .509 | .650 | .430 |
| 2200 | .538 | .670 | .445 |
| 2300 | .568 | .685 | .460 |
| 2400 | .598 | .700 | .470 |
| 2500 | .628 | .720 | .485 |
| 2600 | .656 | .735 | .495 |
| 2700 | .683 | .750 | .505 |
| 2800 | .709 | .770 | .520 |
| 2900 | .735 | .780 | .535 |
| 3000 | .760 | .790 | .555 |
| 3100 | .784 | .805 | .585 |
| 3200 | .807 | .820 | .625 |
| 3300 | .828 | .830 | .700 |
| 3400 | .849 | .840 | .745 |
| 3500 | .869 | .855 | .785 |
| 3600 | .888 | .865 | .810 |
| 3700 | .906 | .875 | .830 |
| 3800 | .922 | .890 | .850 |
| 3900 | .937 | .905 | .870 |
| 4000 | .950 | .925 | .880 |
| 4100 | .962 | .955 | .905 |
| 4300 | .881 | .965 | .915 |
| 4400 | .988 | .975 | .925 |
| 4500 | .993 | .985 | .935 |
| 4600 | .997 | .995 | .940 |
| 4700 | .999 | 1.0 | .945 |
| 4800 | 1.0 | 1.0 | .950 |

Time is time to or time from totality as appropriate.

TABLE A7. PHOTODETACHMENT AND PHOTODISSOCIATION CROSS SECTIONS FOR BENCHMARK-76.

| WAVELENGTH RANGE (NM) | | REACTION NUMBERS | | | | | | | | |
|---|---|---|---|---|---|---|---|---|---|---|
| FROM | TO | 1 | 2 | 3 | 4 | 5 | 6 | 7 | 8 | 9 |
| 100.0 - | 102.6 | 1.000E-18 | 5.200E-18 | 5.500E-18 | 4.000E-18 | 1.000E-18 | 1.400E-18 | 1.000E-17 | 5.000E-20 | 1.000E-18 |
| 102.6 - | 105.3 | 1.000E-18 | 5.200E-18 | 5.500E-18 | 4.000E-18 | 1.000E-18 | 1.400E-18 | 1.000E-17 | 5.000E-20 | 1.000E-18 |
| 105.3 - | 108.1 | 1.000E-18 | 5.200E-18 | 5.500E-18 | 4.000E-18 | 1.000E-18 | 1.400E-18 | 1.000E-17 | 5.000E-20 | 1.000E-18 |
| 108.1 - | 111.1 | 1.000E-18 | 5.200E-18 | 5.500E-18 | 4.000E-18 | 1.000E-18 | 1.400E-18 | 1.000E-17 | 5.000E-20 | 1.000E-18 |
| 111.1 - | 114.3 | 1.000E-18 | 5.200E-18 | 5.600E-18 | 4.000E-18 | 1.000E-18 | 1.400E-18 | 1.000E-17 | 5.000E-20 | 1.000E-18 |
| 114.3 - | 117.6 | 1.000E-18 | 5.200E-18 | 5.600E-18 | 4.000E-18 | 1.000E-18 | 1.400E-18 | 1.000E-17 | 5.000E-20 | 1.000E-18 |
| 117.6 - | 121.2 | 1.000E-18 | 5.200E-18 | 5.600E-18 | 4.000E-18 | 1.000E-18 | 1.400E-18 | 1.000E-17 | 5.000E-20 | 1.000E-18 |
| 121.2 - | 125.0 | 1.000E-18 | 5.200E-18 | 5.700E-18 | 4.000E-18 | 1.000E-18 | 1.400E-18 | 1.000E-17 | 5.000E-20 | 1.000E-18 |
| 125.0 - | 129.0 | 1.000E-18 | 5.200E-18 | 5.700E-18 | 4.000E-18 | 1.000E-18 | 1.400E-18 | 1.000E-17 | 5.000E-20 | 1.000E-18 |
| 129.0 - | 133.3 | 1.000E-18 | 5.200E-18 | 5.800E-18 | 4.000E-18 | 1.000E-18 | 1.400E-18 | 1.000E-17 | 5.000E-20 | 1.000E-18 |
| 133.3 - | 137.9 | 1.000E-18 | 5.300E-18 | 5.900E-18 | 4.000E-18 | 1.000E-18 | 1.400E-18 | 1.000E-17 | 5.000E-20 | 1.000E-18 |
| 137.9 - | 142.9 | 1.000E-18 | 5.300E-18 | 6.000E-18 | 4.000E-18 | 1.000E-18 | 1.400E-18 | 1.000E-17 | 5.000E-20 | 1.000E-18 |
| 142.9 - | 148.1 | 1.000E-18 | 5.300E-18 | 6.100E-18 | 4.000E-18 | 1.000E-18 | 1.400E-18 | 1.000E-17 | 5.000E-20 | 1.000E-18 |
| 148.1 - | 153.8 | 1.000E-18 | 5.300E-18 | 6.300E-18 | 4.000E-18 | 1.000E-18 | 1.400E-18 | 1.000E-17 | 5.000E-20 | 1.000E-18 |
| 153.8 - | 160.0 | 1.000E-18 | 5.400E-18 | 6.400E-18 | 4.000E-18 | 1.000E-18 | 1.400E-18 | 1.000E-17 | 5.000E-20 | 1.000E-18 |
| 160.0 - | 166.7 | 1.000E-18 | 5.400E-18 | 6.500E-18 | 4.000E-18 | 1.000E-18 | 1.400E-18 | 1.000E-17 | 5.000E-20 | 1.000E-18 |
| 166.7 - | 173.9 | 1.000E-18 | 5.400E-18 | 6.700E-18 | 4.000E-18 | 1.000E-18 | 1.400E-18 | 1.000E-17 | 5.000E-20 | 1.000E-18 |
| 173.9 - | 181.8 | 1.000E-18 | 5.500E-18 | 6.900E-18 | 4.000E-18 | 1.000E-18 | 1.400E-18 | 1.000E-17 | 5.000E-20 | 1.000E-18 |
| 181.8 - | 190.5 | 1.000E-18 | 5.500E-18 | 7.300E-18 | 4.000E-18 | 1.000E-18 | 1.400E-18 | 1.000E-17 | 5.000E-20 | 1.000E-18 |
| 190.5 - | 200.0 | 1.000E-18 | 5.600E-18 | 7.500E-18 | 4.000E-18 | 1.000E-18 | 1.400E-18 | 1.000E-17 | 5.000E-20 | 1.000E-18 |
| 200.0 - | 210.5 | 1.000E-18 | 5.700E-18 | 7.700E-18 | 4.000E-18 | 1.000E-18 | 1.400E-18 | 1.000E-17 | 5.000E-20 | 1.000E-18 |
| 210.5 - | 222.2 | 1.000E-18 | 5.800E-18 | 7.600E-18 | 4.000E-18 | 1.000E-18 | 1.400E-18 | 1.000E-17 | 5.000E-20 | 1.000E-18 |
| 222.2 - | 235.3 | 1.000E-18 | 5.800E-18 | 5.900E-18 | 4.000E-18 | 1.000E-18 | 1.400E-18 | 1.000E-17 | 5.000E-20 | 1.000E-18 |
| 235.3 - | 250.0 | 1.000E-18 | 5.900E-18 | 6.000E-18 | 4.000E-18 | 1.000E-18 | 1.400E-18 | 1.000E-17 | 5.000E-20 | 1.000E-18 |
| 250.0 - | 266.7 | 1.000E-18 | 6.000E-18 | 6.200E-18 | 4.000E-18 | 1.000E-18 | 1.400E-18 | 1.000E-17 | 5.000E-20 | 1.000E-18 |
| 266.7 - | 285.7 | 1.000E-18 | 6.000E-18 | 6.500E-18 | 4.000E-18 | 1.000E-18 | 1.400E-18 | 1.000E-17 | 5.000E-20 | 1.000E-18 |
| 285.7 - | 307.7 | 1.000E-18 | 6.100E-18 | 6.700E-18 | 4.000E-18 | 1.000E-18 | 1.400E-18 | 1.000E-17 | 5.000E-20 | 1.000E-18 |
| 307.7 - | 333.3 | 1.000E-18 | 6.200E-18 | 6.600E-18 | 4.000E-18 | 1.000E-18 | 1.400E-18 | 1.000E-17 | 5.000E-20 | 1.000E-18 |
| 333.3 - | 363.6 | 1.000E-18 | 6.200E-18 | 4.800E-18 | 3.500E-18 | 1.000E-18 | 1.400E-18 | 1.000E-17 | 5.000E-20 | 1.000E-18 |
| 363.6 - | 400.0 | 1.000E-18 | 6.300E-18 | 0. | 2.900E-18 | 9.000E-19 | 1.400E-18 | 1.000E-17 | 5.000E-20 | 1.000E-18 |
| 400.0 - | 430.0 | 8.000E-19 | 6.300E-18 | 0. | 2.400E-18 | 9.000E-19 | 1.400E-18 | 1.000E-17 | 5.000E-20 | 1.000E-18 |
| 430.0 - | 470.0 | 2.000E-19 | 6.300E-18 | 0. | 2.200E-18 | 9.000E-19 | 1.200E-18 | 1.000E-17 | 5.000E-20 | 1.000E-18 |
| 470.0 - | 510.0 | 1.000E-20 | 6.300E-18 | 0. | 1.800E-18 | 8.000E-19 | 7.000E-19 | 1.000E-17 | 5.000E-20 | 1.000E-18 |
| 510.0 - | 560.0 | 0. | 6.300E-18 | 0. | 1.500E-18 | 3.000E-19 | 1.300E-18 | 1.000E-17 | 5.000E-20 | 1.000E-18 |
| 560.0 - | 620.0 | 0. | 6.200E-18 | 0. | 1.300E-18 | 3.000E-20 | 1.400E-18 | 1.000E-17 | 5.000E-20 | 1.000E-18 |
| 620.0 - | 680.0 | 0. | 5.800E-18 | 0. | 1.100E-18 | 0. | 1.500E-18 | 1.000E-17 | 1.200E-19 | 1.000E-18 |
| 680.0 - | 730.0 | 0. | 5.400E-18 | 0. | 9.000E-19 | 0. | 2.000E-19 | 1.000E-17 | 1.200E-19 | 1.000E-18 |

PHOTODISSOCIATION CROSSECTIONS (CM**2) USED IN SUBPROGRAM BLKDAT - 76/12/16

| WAVELENGTH RANGE (NM) | | REACTION NUMBERS | | | | | | | |
|---|---|---|---|---|---|---|---|---|---|
| FROM | TO | 10 | 11 | 12 | 13 | 14 | 15 | 16 | 17 |
| 100.0 - | 102.6 | 1.000E-18 | 1.000E-18 | 1.000E-18 | 1.000E-18 | 1.000E-18 | 1.000E-18 | 5.000E-18 | 2.000E-18 |
| 102.6 - | 105.3 | 1.000E-18 | 1.000E-18 | 1.000E-18 | 1.000E-18 | 1.000E-18 | 1.000E-18 | 5.000E-18 | 2.000E-18 |
| 105.3 - | 108.1 | 1.000E-18 | 1.000E-18 | 1.000E-18 | 1.000E-18 | 1.000E-18 | 1.000E-18 | 5.000E-18 | 2.000E-18 |
| 108.1 - | 111.1 | 1.000E-18 | 1.000E-18 | 1.000E-18 | 1.000E-18 | 1.000E-18 | 1.000E-18 | 5.000E-18 | 2.000E-18 |
| 111.1 - | 114.3 | 1.000E-18 | 1.000E-18 | 1.000E-18 | 1.000E-18 | 1.000E-18 | 1.000E-18 | 5.000E-18 | 2.000E-18 |
| 114.3 - | 117.6 | 1.000E-18 | 1.000E-18 | 1.000E-18 | 1.000E-18 | 1.000E-18 | 1.000E-18 | 5.000E-18 | 2.000E-18 |
| 117.6 - | 121.2 | 1.000E-18 | 1.000E-18 | 1.000E-18 | 1.000E-18 | 1.000E-18 | 1.000E-18 | 5.000E-18 | 2.000E-18 |
| 121.2 - | 125.0 | 1.000E-18 | 1.000E-18 | 1.000E-18 | 1.000E-18 | 1.000E-18 | 1.000E-18 | 5.000E-18 | 2.000E-18 |
| 125.0 - | 129.0 | 1.000E-18 | 1.000E-18 | 1.000E-18 | 1.000E-18 | 1.000E-18 | 1.000E-18 | 5.000E-18 | 2.000E-18 |
| 129.0 - | 133.3 | 1.000E-18 | 1.000E-18 | 1.000E-18 | 1.000E-18 | 1.000E-18 | 1.000E-18 | 5.000E-18 | 2.000E-18 |
| 133.3 - | 137.9 | 1.000E-18 | 1.000E-18 | 1.000E-18 | 1.000E-18 | 1.000E-18 | 1.000E-18 | 5.000E-18 | 2.000E-18 |
| 137.9 - | 142.9 | 1.000E-18 | 1.000E-18 | 1.000E-18 | 1.000E-18 | 1.000E-18 | 1.000E-18 | 5.000E-18 | 2.000E-18 |
| 142.9 - | 148.1 | 1.000E-18 | 1.000E-18 | 1.000E-18 | 1.000E-18 | 1.000E-18 | 1.000E-18 | 5.000E-18 | 2.000E-18 |
| 148.1 - | 153.8 | 1.000E-18 | 1.000E-18 | 1.000E-18 | 1.000E-18 | 1.000E-18 | 1.000E-18 | 5.000E-18 | 2.000E-18 |
| 153.8 - | 160.0 | 1.000E-18 | 1.000E-18 | 1.000E-18 | 1.000E-18 | 1.000E-18 | 1.000E-18 | 5.000E-18 | 2.000E-18 |
| 160.0 - | 166.7 | 1.000E-18 | 1.000E-18 | 1.000E-18 | 1.000E-18 | 1.000E-18 | 1.000E-18 | 5.000E-18 | 2.000E-18 |
| 166.7 - | 173.9 | 1.000E-18 | 1.000E-18 | 1.000E-18 | 1.000E-18 | 1.000E-18 | 1.000E-18 | 5.000E-18 | 2.000E-18 |
| 173.9 - | 181.8 | 1.000E-18 | 1.000E-18 | 1.000E-18 | 1.000E-18 | 1.000E-18 | 1.000E-18 | 5.000E-18 | 2.000E-18 |
| 181.8 - | 190.5 | 1.000E-18 | 1.000E-18 | 1.000E-18 | 1.000E-18 | 1.000E-18 | 1.000E-18 | 5.000E-18 | 2.000E-18 |
| 190.5 - | 200.0 | 1.000E-18 | 1.000E-18 | 1.000E-18 | 1.000E-18 | 1.000E-18 | 1.000E-18 | 5.000E-18 | 2.000E-18 |
| 200.0 - | 210.5 | 1.000E-18 | 1.000E-18 | 1.000E-18 | 1.000E-18 | 1.000E-18 | 1.000E-18 | 5.000E-18 | 2.000E-18 |
| 210.5 - | 222.2 | 1.000E-18 | 1.000E-18 | 1.000E-18 | 1.000E-18 | 1.000E-18 | 1.000E-18 | 5.000E-18 | 2.000E-18 |
| 222.2 - | 235.3 | 1.000E-18 | 1.000E-18 | 1.000E-18 | 1.000E-18 | 1.000E-18 | 1.000E-18 | 5.000E-18 | 2.000E-18 |
| 235.3 - | 250.0 | 1.000E-18 | 1.000E-18 | 1.000E-18 | 1.000E-18 | 1.000E-18 | 1.000E-18 | 5.000E-18 | 2.000E-18 |
| 250.0 - | 266.7 | 1.000E-18 | 1.000E-18 | 1.000E-18 | 1.000E-18 | 1.000E-18 | 1.000E-18 | 5.000E-18 | 2.000E-18 |
| 266.7 - | 285.7 | 1.000E-18 | 8.000E-19 | 1.000E-18 | 1.000E-18 | 1.000E-18 | 1.000E-18 | 5.000E-18 | 2.000E-18 |
| 285.7 - | 307.7 | 1.000E-18 | 3.000E-19 | 1.000E-18 | 1.000E-18 | 1.000E-18 | 1.000E-18 | 5.000E-18 | 2.000E-18 |
| 307.7 - | 333.3 | 1.000E-18 | 1.000E-19 | 1.000E-18 | 1.000E-18 | 1.000E-18 | 1.000E-18 | 5.000E-18 | 2.000E-18 |
| 333.3 - | 363.6 | 1.000E-18 | 1.000E-20 | 1.000E-18 | 1.000E-18 | 1.000E-18 | 1.000E-18 | 5.000E-18 | 2.000E-18 |
| 363.6 - | 400.0 | 1.000E-18 | 0. | 1.000E-18 | 1.000E-18 | 1.000E-18 | 1.000E-18 | 5.000E-18 | 2.000E-18 |
| 400.0 - | 430.0 | 1.000E-18 | 0. | 1.000E-18 | 1.000E-18 | 1.000E-18 | 1.000E-18 | 5.000E-18 | 2.000E-18 |
| 430.0 - | 470.0 | 1.000E-18 | 0. | 1.000E-18 | 1.000E-18 | 1.000E-18 | 1.000E-18 | 5.000E-18 | 2.000E-18 |
| 470.0 - | 510.0 | 1.000E-18 | 0. | 1.000E-18 | 1.000E-18 | 1.000E-18 | 1.000E-18 | 6.000E-18 | 2.000E-18 |
| 510.0 - | 560.0 | 1.000E-18 | 0. | 0. | 1.000E-18 | 1.000E-18 | 1.000E-18 | 3.000E-18 | 1.800E-18 |
| 560.0 - | 620.0 | 1.000E-18 | 0. | 0. | 1.000E-18 | 1.000E-18 | 5.000E-19 | 1.000E-18 | 1.800E-18 |
| 620.0 - | 680.0 | 1.000E-18 | 0. | 0. | 1.000E-18 | 1.000E-18 | 2.000E-19 | 1.500E-19 | 1.000E-18 |
| 680.0 - | 730.0 | 1.000E-18 | 0. | 0. | 1.000E-18 | 1.000E-18 | 5.000E-20 | 0. | 0. |

PHOTODISSOCIATION CROSSECTIONS (CM**2) USED IN SUBPROGRAM BLKDAT - 76/12/16

| WAVELENGTH RANGE (NM) | | REACTION NUMBERS | | | | | | | | |
|---|---|---|---|---|---|---|---|---|---|---|
| FROM | TO | 33 | 34 | 35 | 36 | 37 | 38 | 39 | 40 | 41 |
| 100.0 - | 102.6 | 1.000E-18 | 8.000E-18 | 1.000E-18 | 1.000E-20 | 1.000E-18 | 1.000E-18 | 1.040E-17 | 1.000E-18 | 0. |
| 102.6 - | 105.3 | 1.000E-18 | 4.000E-18 | 1.000E-18 | 1.000E-20 | 1.000E-18 | 1.000E-18 | 5.100E-18 | 1.000E-18 | 0. |
| 105.3 - | 108.1 | 1.000E-18 | 6.000E-18 | 1.000E-18 | 1.000E-20 | 1.000E-18 | 1.000E-18 | 3.100E-18 | 1.000E-18 | 0. |
| 108.1 - | 111.1 | 1.000E-18 | 5.000E-18 | 1.000E-18 | 1.000E-20 | 1.000E-18 | 1.000E-18 | 1.200E-18 | 9.000E-18 | 0. |
| 111.1 - | 114.3 | 0. | 1.000E-18 | 1.000E-18 | 1.000E-20 | 1.000E-18 | 1.000E-18 | 7.000E-19 | 8.200E-18 | 0. |
| 114.3 - | 117.6 | 0. | 1.000E-18 | 1.000E-18 | 1.000E-20 | 1.000E-18 | 1.000E-18 | 4.000E-19 | 7.000E-18 | 0. |
| 117.6 - | 121.2 | 0. | 1.000E-18 | 1.000E-18 | 1.000E-20 | 1.000E-18 | 1.000E-18 | 3.000E-19 | 7.300E-18 | 0. |
| 121.2 - | 125.0 | 0. | 6.000E-18 | 1.000E-18 | 1.000E-20 | 1.000E-18 | 1.000E-18 | 4.000E-19 | 1.100E-17 | 0. |
| 125.0 - | 129.0 | 0. | 7.000E-18 | 1.000E-18 | 1.000E-20 | 1.000E-18 | 1.000E-18 | 1.100E-18 | 1.500E-17 | 0. |
| 129.0 - | 133.3 | 0. | 6.000E-18 | 1.000E-18 | 1.000E-20 | 1.000E-18 | 1.000E-18 | 1.900E-18 | 1.100E-17 | 0. |
| 133.3 - | 137.9 | 0. | 3.000E-18 | 1.000E-18 | 1.000E-20 | 1.000E-18 | 1.000E-18 | 2.000E-18 | 9.300E-18 | 0. |
| 137.9 - | 142.9 | 0. | 7.000E-19 | 1.000E-18 | 1.000E-20 | 1.000E-18 | 1.000E-18 | 2.500E-18 | 1.300E-17 | 0. |
| 142.9 - | 148.1 | 0. | 6.000E-19 | 1.000E-18 | 1.000E-20 | 1.000E-18 | 1.000E-18 | 2.500E-18 | 1.300E-17 | 0. |
| 148.1 - | 153.8 | 0. | 1.200E-18 | 1.000E-18 | 1.000E-20 | 1.000E-18 | 1.000E-18 | 1.200E-18 | 1.300E-17 | 0. |
| 153.8 - | 160.0 | 0. | 2.000E-18 | 1.000E-18 | 1.000E-20 | 1.000E-18 | 1.000E-18 | 3.000E-19 | 1.500E-17 | 0. |
| 160.0 - | 166.7 | 0. | 4.500E-18 | 1.000E-18 | 1.000E-20 | 1.000E-18 | 1.000E-18 | 2.000E-19 | 1.500E-17 | 0. |
| 166.7 - | 173.9 | 0. | 3.200E-18 | 1.000E-18 | 1.000E-20 | 1.000E-18 | 1.000E-18 | 1.500E-19 | 1.500E-17 | 0. |
| 173.9 - | 181.8 | 0. | 3.000E-19 | 1.000E-18 | 1.000E-20 | 1.000E-18 | 1.000E-18 | 2.000E-19 | 1.000E-17 | 0. |
| 181.8 - | 190.5 | 0. | 5.000E-21 | 1.000E-18 | 1.000E-20 | 1.000E-18 | 3.800E-18 | 1.500E-19 | 2.200E-18 | 0. |
| 190.5 - | 200.0 | 0. | 6.000E-23 | 6.000E-19 | 1.000E-20 | 9.100E-18 | 4.300E-18 | 0. | 4.200E-19 | 0. |
| 200.0 - | 210.5 | 0. | 0. | 4.600E-19 | 1.000E-20 | 2.500E-18 | 4.600E-18 | 0. | 4.000E-19 | 0. |
| 210.5 - | 222.2 | 0. | 0. | 3.300E-19 | 1.000E-20 | 2.500E-19 | 4.200E-18 | 0. | 4.500E-19 | 0. |
| 222.2 - | 235.3 | 0. | 0. | 2.200E-19 | 1.000E-20 | 7.000E-20 | 2.900E-18 | 0. | 2.500E-19 | 0. |
| 235.3 - | 250.0 | 0. | 0. | 1.200E-19 | 1.000E-20 | 2.400E-20 | 1.100E-18 | 0. | 5.400E-20 | 0. |
| 250.0 - | 266.7 | 0. | 0. | 7.000E-20 | 1.000E-20 | 1.900E-20 | 4.000E-19 | 0. | 1.900E-20 | 0. |
| 266.7 - | 285.7 | 0. | 0. | 3.000E-20 | 1.000E-20 | 1.400E-20 | 1.000E-19 | 0. | 5.100E-20 | 0. |
| 285.7 - | 307.7 | 0. | 0. | 1.200E-20 | 8.300E-21 | 4.000E-21 | 0. | 0. | 1.200E-19 | 0. |
| 307.7 - | 333.3 | 0. | 0. | 5.000E-21 | 1.900E-20 | 2.000E-22 | 0. | 0. | 3.000E-19 | 0. |
| 333.3 - | 363.6 | 0. | 0. | 2.000E-21 | 4.200E-20 | 0. | 0. | 0. | 5.100E-19 | 0. |
| 363.6 - | 400.0 | 0. | 0. | 3.000E-22 | 3.100E-20 | 0. | 0. | 0. | 6.300E-19 | 0. |
| 400.0 - | 430.0 | 0. | 0. | 0. | 0. | 0. | 0. | 0. | 6.000E-20 | 0. |
| 430.0 - | 470.0 | 0. | 0. | 0. | 0. | 0. | 0. | 0. | 0. | 0. |
| 470.0 - | 510.0 | 0. | 0. | 0. | 0. | 0. | 0. | 0. | 0. | 0. |
| 510.0 - | 560.0 | 0. | 0. | 0. | 0. | 0. | 0. | 0. | 0. | 0. |
| 560.0 - | 620.0 | 0. | 0. | 0. | 0. | 0. | 0. | 0. | 0. | 0. |
| 620.0 - | 680.0 | 0. | 0. | 0. | 0. | 0. | 0. | 0. | 0. | 0. |
| 680.0 - | 730.0 | 0. | 0. | 0. | 0. | 0. | 0. | 0. | 0. | 0. |

PHOTODISSOCIATION CROSSECTIONS (CM**2) USED IN SUBPROGRAM BLKDAT - 76/12/16

| WAVELENGTH RANGE (NM) | | REACTION NUMBERS | | | | | | | |
|---|---|---|---|---|---|---|---|---|---|
| FROM | TO | 42 | 43 | 44 | 45 | 46 | 47 | 48 | 49 |
| 100.0 - | 102.6 | 1.000E-18 | 0. | 4.000E-19 | 0. | 0. | 0. | 0. | 1.000E-18 |
| 102.6 - | 105.3 | 1.000E-18 | 0. | 1.000E-18 | 0. | 0. | 0. | 0. | 1.000E-18 |
| 105.3 - | 108.1 | 1.000E-18 | 0. | 5.000E-20 | 0. | 0. | 0. | 0. | 9.300E-18 |
| 108.1 - | 111.1 | 3.700E-17 | 0. | 4.300E-21 | 0. | 0. | 0. | 0. | 9.300E-18 |
| 111.1 - | 114.3 | 2.600E-17 | 0. | 1.000E-20 | 0. | 0. | 0. | 0. | 1.040E-17 |
| 114.3 - | 117.6 | 1.100E-17 | 0. | 1.000E-20 | 0. | 0. | 0. | 0. | 6.700E-18 |
| 117.6 - | 121.2 | 3.700E-18 | 0. | 7.000E-21 | 0. | 0. | 0. | 0. | 9.300E-18 |
| 121.2 - | 125.0 | 5.600E-18 | 0. | 1.000E-20 | 0. | 0. | 0. | 0. | 1.500E-17 |
| 125.0 - | 129.0 | 7.100E-17 | 0. | 6.500E-20 | 0. | 0. | 0. | 0. | 7.100E-18 |
| 129.0 - | 133.3 | 5.600E-17 | 0. | 1.000E-18 | 0. | 0. | 0. | 0. | 1.300E-17 |
| 133.3 - | 137.9 | 2.600E-18 | 0. | 6.000E-18 | 0. | 0. | 0. | 0. | 9.300E-18 |
| 137.9 - | 142.9 | 1.700E-18 | 0. | 1.400E-17 | 0. | 0. | 0. | 0. | 7.400E-18 |
| 142.9 - | 148.1 | 6.300E-18 | 0. | 1.400E-17 | 0. | 0. | 0. | 0. | 5.600E-18 |
| 148.1 - | 153.8 | 9.300E-19 | 0. | 1.200E-17 | 0. | 0. | 0. | 0. | 3.300E-18 |
| 153.8 - | 160.0 | 7.800E-20 | 0. | 8.000E-18 | 0. | 0. | 0. | 0. | 1.120E-18 |
| 160.0 - | 166.7 | 4.800E-20 | 0. | 3.500E-18 | 0. | 0. | 0. | 0. | 9.300E-19 |
| 166.7 - | 173.9 | 8.900E-20 | 0. | 3.000E-19 | 0. | 0. | 0. | 0. | 8.200E-19 |
| 173.9 - | 181.8 | 1.400E-19 | 3.000E-22 | 3.000E-22 | 0. | 0. | 0. | 0. | 7.400E-19 |
| 181.8 - | 190.5 | 1.300E-19 | 1.200E-23 | 1.200E-23 | 0. | 0. | 0. | 0. | 6.700E-19 |
| 190.5 - | 200.0 | 8.000E-20 | 1.200E-23 | 1.200E-23 | 0. | 0. | 0. | 0. | 4.100E-19 |
| 200.0 - | 210.5 | 1.500E-20 | 9.000E-24 | 9.000E-24 | 0. | 0. | 0. | 0. | 3.300E-19 |
| 210.5 - | 222.2 | 1.500E-21 | 1.000E-23 | 1.000E-23 | 0. | 0. | 0. | 0. | 1.100E-18 |
| 222.2 - | 235.3 | 1.000E-22 | 5.000E-24 | 5.000E-24 | 0. | 0. | 0. | 0. | 4.000E-18 |
| 235.3 - | 250.0 | 1.300E-23 | 1.000E-24 | 1.000E-24 | 0. | 0. | 0. | 0. | 9.200E-18 |
| 250.0 - | 266.7 | 5.000E-24 | 0. | 0. | 0. | 0. | 0. | 0. | 1.100E-17 |
| 266.7 - | 285.7 | 6.000E-24 | 0. | 0. | 0. | 0. | 0. | 0. | 5.600E-18 |
| 285.7 - | 307.7 | 4.000E-24 | 0. | 0. | 0. | 0. | 0. | 0. | 6.000E-19 |
| 307.7 - | 333.3 | 1.000E-24 | 0. | 0. | 0. | 0. | 0. | 2.000E-20 | 0. |
| 333.3 - | 363.6 | 0. | 0. | 0. | 0. | 0. | 0. | 5.000E-22 | 0. |
| 363.6 - | 400.0 | 0. | 0. | 0. | 0. | 0. | 0. | 0. | 0. |
| 400.0 - | 430.0 | 0. | 0. | 0. | 0. | 0. | 4.140E-23 | 0. | 0. |
| 430.0 - | 470.0 | 0. | 0. | 0. | 0. | 0. | 1.920E-22 | 0. | 0. |
| 470.0 - | 510.0 | 0. | 0. | 0. | 0. | 0. | 8.780E-22 | 0. | 0. |
| 510.0 - | 560.0 | 0. | 0. | 0. | 0. | 0. | 2.480E-21 | 0. | 0. |
| 560.0 - | 620.0 | 0. | 0. | 0. | 0. | 0. | 4.250E-21 | 0. | 0. |
| 620.0 - | 680.0 | 0. | 0. | 0. | 0. | 0. | 2.650E-21 | 0. | 0. |
| 680.0 - | 730.0 | 0. | 0. | 0. | 0. | 0. | 8.900E-22 | 0. | 0. |

TABLE A8. PHOTOLYTIC REACTIONS AND REFERENCES FOR BENCHMARK-76.

| REAC. NO. | REACTION | WAVELENGTH REGION | REFERENCE | REF. NO. |
|---|---|---|---|---|
| 1 | NO2- + HV = NO2 + E | 100-430 NM, BANDS 11-41 | ESTIMATED, SEE TEXT | 1 |
| | | 430-560 NM, BANDS 42-44 | HERRST ET AL, JCP V61 P1300-4 FIG 3, 1974 BUT SEE TEXT | 1 |
| 2 | O- + HV = O + E | 100-116 NM, BANDS 11-16 | EXTRAPOLATION FROM CHURCHILL, SEE TEXT | 2 |
| | | 116-730 NM, BANDS 16-47 | CHURCHILL ET AL, JQSRT V6, P371-442 1966 | 2 |
| 3 | O- + HV = O1D + E | 100-116 NM, BANDS 11-16 | EXTRAPOLATION FROM CHURCHILL, SEE TEXT | 3 |
| | | 116-730 NM, BANDS 16-47 | CHURCHILL ET AL, JQSRT V6, P371-442 1966 | 3 |
| 4 | O2- + HV = O2 + E | 100-450 NM, BANDS 11-41 | ESTIMATED, SEE TEXT | 4 |
| | | 440-730 NM, BANDS 42-47 | BURCH ET AL, PHYS REV V112 P 171 1958 | 4 |
| | | 440-730 NM, BANDS 42-47 | BURCH ET AL, PHYS REV V114 P 1652, 1959 | 4 |
| 5 | O3- + HV = O3 + E | 100-450 NM, BANDS 11-42 | ESTIMATED, SEE TEXT | 5 |
| | | 440-730 NM, BANDS 43-46 | COSBY ET AL, JCP V63 P1612-20 1975 | 5 |
| 6 | CO3- + HV = CO2 + O- | 100-450 NM, BANDS 11-42 | ESTIMATED, SEE TEXT | 6 |
| | | 450-560 NM, BANDS 43-44 | MOSELEY ET AL, JCP V65, P2512-7 1976 | 6 |
| | | 560-740 NM, BANDS 45-47 | PETERSON, JGR V81 P1433-5 1975 | 6 |
| 7 | 78- + HV = CO3- + H2O | 100-560 NM, BANDS 11-44 | ESTIMATED, SEE TEXT | 7 |
| | | 560-700 NM, BANDS 45-47 | PETERSON JGR V81 P1433-5 1975 | 7 |
| 8 | CO4- + HV = O2- + CO2 | 100-510 NM, BANDS 11-43 | ESTIMATED, SEE TEXT | 8 |
| | | 510-680 NM, BANDS 44-46 | J MOSELEY, JCP V65 N12 P5267-74 1976 | 8 |
| | | 680-740 NM, BAND 47 | ESTIMATED, SEE TEXT | 8 |
| 9 | 94- + HV = CO4- + H2O | 100-740 NM, BANDS 11-47 | ESTIMATED, SEE TEXT | 9 |
| 10 | 64- + HV = NO2- + H2O | 100-740 NM, BANDS 11-47 | ESTIMATED, SEE TEXT | 10 |
| 11 | NO3- + HV = O + NO2 + E | 100-267 NM, BANDS 11-35 | ESTIMATED, SEE TEXT | 11 |
| | | 267-364 NM, BANDS 36-39 | ESTIMATED, SEE TEXT, USED NO2- SHAPE SHIFTED | 11 |
| 12 | 62- + HV = NO + O2- | 100-740 NM, BANDS 11-47 | ESTIMATED, SEE TEXT, NO3- ISOMER | 12 |
| 13 | 80- + HV = NO3- + H2O | 100-740 NM, BANDS 11-47 | ESTIMATED, SEE TEXT | 13 |
| 14 | 125- + HV = NO3- + HNO3 | 100-740 NM, BANDS 11-47 | ESTIMATED, SEE TEXT | 14 |
| 15 | O2-W + HV = O2- + H2O | 100-560 NM, BANDS 11-44 | ESTIMATED, SEE TEXT | 15 |
| | | 560-670 NM, BANDS 45-46 | J MOSELEY, JCP V65 N12 P5267-74 1976 | 15 |
| 16 | O3- + HV = O- + O2 | 680-740 NM, BAND 47 | ESTIMATE, SEE TEXT | 15 |
| | | 100-440 NM, BANDS 11-42 | ESTIMATED, SEE TEXT | 16 |
| 17 | O4- + HV = O2- + O2 | 440-640 NM, BANDS 43-46 | COSBY ET AL, JCP V63 P1612-1620, 1975 | 16 |
| | | 100-440 NM, BANDS 11-43 | ESTIMATED, SEE TEXT | 17 |
| 18 | NO74 + HV = NO+ + CO2 | 450-650 NM, BANDS 43-46 | COSBY ET AL JCP V63 P1612-1620 1975 | 17 |
| 19 | NO48 + HV = NO+ + H2O | | NOT COMPUTED AT THIS TIME | 18 |
| 20 | NO58 + HV = NO+ + N2 | | NOT COMPUTED AT THIS TIME | 19 |
| 21 | NO92 + HV = NO48 + CO2 | | NOT COMPUTED AT THIS TIME | 20 |
| 22 | NO66 + HV = H3O+ + HNO2 | | NOT COMPUTED AT THIS TIME | 21 |
| 23 | NO66 + HV = NO48 + H2O | | NOT COMPUTED AT THIS TIME | 22 |
| 24 | NO76 + HV = NO48 + N2 | | NOT COMPUTED AT THIS TIME | 23 |
| 25 | N110 + HV = NO66 + CO2 | | NOT COMPUTED AT THIS TIME | 24 |
| 26 | NO84 + HV = NO66 + H2O | | NOT COMPUTED AT THIS TIME | 25 |
| 27 | NO94 + HV = NO66 + N2 | | NOT COMPUTED AT THIS TIME | 26 |
| 28 | 64+ + HV = NO2+ + H2O | | NOT COMPUTED AT THIS TIME | 27 |
| 29 | 82+ + HV = 64+ + H2O | | NOT COMPUTED AT THIS TIME | 28 |
| 30 | O2S0 + HV = O2+ + H2O | | NOT COMPUTED AT THIS TIME | 29 |
| 31 | O260 + HV = O2+ + N2 | | NOT COMPUTED AT THIS TIME | 30 |
| 32 | O4+ + HV = O2+ + O2 | | NOT COMPUTED AT THIS TIME | 31 |
| 33 | H2 + HV = H + H | | NOT COMPUTED AT THIS TIME | 32 |
| 34 | H2O + HV = H + HO | 100-111 NM, BANDS 11-14 | ESTIMATED, SEE TEXT | 33 |
| | | 100-111 NM, BANDS 11-14 | R D HUDSON, RGP+SP V9 P305-406 1971 | 34 |
| 35 | H2O2 + HV = HO + HO | 111-121 NM, BANDS 15-17 | ESTIMATED, SEE TEXT | 34 |
| | | 121-190 NM, BANDS 18-29 | R D HUDSON + DNA 1984H RRH REV 1972 | 34 |
| 36 | HNO2 + HV = HO + NO | 190-200 NM, BAND 30 | THOMPSON ET AL, ADV PHOTOCHEM V3, P192 | 34 |
| | | 100-125 NM, BANDS 11-18 | ESTIMATED, SEE TEXT | 35 |
| 37 | HNO3 + HV = HO + NO2 | 125-142 NM, BANDS 19-22 | HAMPSON JPCRD V2 P290-291 1973 | 35 |
| | | 138-200 NM, BANDS 22-30 | URFY ET AL JACS V51 P1371-83 1929 | 35 |
| | | 100-286 NM, BANDS 11-36 | ESTIMATED, SEE TEXT | 36 |
| | | 286-400 NM, BANDS 37-40 | JOHNSTON + GRAHAM CAN J CHEM V52 P1415-23 1974 | 36 |
| | | 100-125 NM, BANDS 11-18 | ESTIMATED, SEE TEXT | 37 |

| REAC. NO. | REACTION | WAVELENGTH REGION | REFERENCE | REF. NO. |
|---|---|---|---|---|
| 38 | $HO_2 + HV = HO + O$ | 125-167 NM, BANDS 19-26 | JOHNSTON + GRAHAM CAN J CHEM V52 P1415-23 1974 | 37 |
| | | 100-125 NM, BANDS 11-18 | ESTIMATED, SEE TEXT | 38 |
| | | 125-167 NM, BANDS 19-26 | J TROE IN NBSIR-73-206, GARVIN ED. 1973 | 38 |
| 39 | $NO + HV = N + O$ | 100-191 NM, BANDS 11-29 | DNA 1948H RRH REV 1972 | 39 |
| 40 | $NO_2 + HV = NO + O$ | 100-108 NM, BANDS 11-13 | ESTIMATED, SEE TEXT | 40 |
| | | 108-190 NM, BANDS 14-29 | NBSIR 73-207 GARVIN, ED. 1973 | 40 |
| | | 190-286 NM, BANDS 30-36 | JOHNSTON + GRAHAM CAN J CHEM V52 P1415-23 1974 | 40 |
| | | 286-400 NM, BANDS 37-40 | NBSIR 73-207 GARVIN ED 1973 | 40 |
| 41 | $N_2 + HV = N_2O + N$ | | NOT COMPUTED AT THIS TIME | 41 |
| 42 | $N_2O + HV = N_2 + O1D$ | 100-108 NM, BANDS 11-13 | ESTIMATED, SEE TEXT | 42 |
| | | 108-182 NM, BANDS 14-28 | ZELIKOFF ET AL JCP V21 P1643-7 1953 | 42 |
| | | 182-333 NM, BANDS 29-38 | JOHNSTON + GRAHAM CAN J CHEM V52 P1415-23 1974 | 42 |
| 43 | $O_2 + HV = O + O$ | | SEE TEXT FOR SQUARE ROOT LAW | 43 |
| | | 174-250 NM, BANDS 28-34 | ACKERMAN ET AL PLNT + SPA SCI V18 P1639-51 1970 | 43 |
| 44 | $O_2 + HV = O + O1D$ | | SEE TEXT FOR SQUARE ROOT LAW | 44 |
| | | 100-111 NM, BANDS 11-14 | D M HUNTEN + M B MCELROY JGR V73 P2421-8 1968 | 44 |
| | | 111-129 NM, BANDS 14-19 | R D HUDSON RGP+SP V9 P305-406 1971 | 44 |
| 45 | $O_2 + HV = O2ID$ | 125-174 NM BANDS 19-27 | BLAKE ET AL JQSRT V6 PP451-9 FIG5 1966 | 44 |
| 46 | $O_2 + HV = O2IS$ | | NOT COMPUTED AT THIS TIME | 45 |
| 47 | $O_3 + HV = O + O_2$ | | NOT COMPUTED AT THIS TIME | 46 |
| 48 | $O_3 + HV = O + O2ID$ | 400-730 NM, BANDS 41-47 | JOHNSTON + GRAHAM CAN J CH V52 P1415-23 1974 | 47 |
| 49 | $O_3 + HV = O1D + O2ID$ | 308-364 NM, BANDS 38-39 | R D HUDSON RGP+SP V9 P305-406 1971 | 48 |
| | | 100-105 NM, BANDS 11-12 | ESTIMATED, SEE TEXT | 49 |
| 50 | $N + HV = N+ + E$ | 105-222 NM, BANDS 13-32 | Y TANAKA ET AL J C P V21 P1651-53 1953 | 49 |
| | | 200-308 NM, BANDS 31-37 | R D HUDSON RGP+SP V9 P305-406 1971 | 49 |
| 51 | $NO + HV = NO+ + E$ | 0.4-10 NM, BANDS 1-10 | W SWIDER RGP+SP V7 P573-94, 1969 | 50 |
| | | GAMMA- X-RAY PRE ELECT | SEE IONIZATION SECTION OF TEXT | 50 |
| 52 | $NO_2 + HV = NO_2+ + E$ | 0.4-10 NM, BANDS 1-10 | W SWIDER RGP+SP V7 P573-94, 1969 | 51 |
| | | GAMMA- X-RAY PRE ELECT | SEE IONIZATION SECTION OF TEXT | 51 |
| | | 100-114 NM, BANDS 11-15 | WATANABE ET AL APLD OPT V6 P391-6, P1220 1967 | 51 |
| | | 114-133 NM, BANDS 16-20 | DNA 1948H RRH 1972 | 51 |
| 53 | $N_2 + HV = N + N+ + E$ | 0.4-10 NM, BANDS 1-10 | W SWIDER RGP+SP V7 P573-94, 1969 | 52 |
| | | GAMMA- X-RAY PRE ELECT | SEE IONIZATION SECTION OF TEXT | 52 |
| 54 | $N_2 + HV = N2D + N+ + E$ | 100-114 NM, BANDS 11-14 | ESTIMATED | 52 |
| 55 | $N_2 + HV = N_2+ + E$ | 114-129 NM, BANDS 15-19 | NAKAYAMA ET AL JCP V30 P1180-6 1959 | 52 |
| | | 0.4-10 NM, BANDS 1-10 | W SWIDER RGP+SP V7 P573-94, 1969 | 53 |
| 56 | $O + HV = O+ + E$ | GAMMA- X-RAY PRE ELECT | SEE IONIZATION SECTION OF TEXT | 53 |
| | | | NOT COMPUTED AT THIS TIME | 54 |
| 57 | $O_2 + HV = O_2+ + E$ | 0.4-10 NM, BANDS 1-10 | W SWIDER RGP+SP V7 P573-94, 1969 | 55 |
| | | GAMMA- X-RAY PRE ELECT | SEE IONIZATION SECTION OF TEXT | 55 |
| 58 | $O_2 + HV = O + O+ + E$ | 0.4-10 NM, BANDS 1-10 | W SWIDER RGP+SP V7 P573-94, 1969 | 56 |
| | | GAMMA- X-RAY PRE ELECT | SEE IONIZATION SECTION OF TEXT | 56 |
| 59 | $O_2 + HV = O1D + O+ + E$ | 0.4-10 NM, BANDS 1-10 | W SWIDER RGP+SP V7 P573-94, 1969 | 57 |
| 60 | $O2ID + HV = O_2+ + E$ | GAMMA- X-RAY PRE ELECT | SEE IONIZATION SECTION OF TEXT | 57 |
| | | 100-103 NM, BAND 11 | DNA 1948H RRH 1972 | 57 |
| | | 0.4-10 NM, BANDS 1-10 | W SWIDER RGP+SP V7 P573-94, 1969 | 58 |
| | | GAMMA- X-RAY PRE ELECT | SEE IONIZATION SECTION OF TEXT | 58 |
| | | | NOT COMPUTED AT THIS TIME | 59 |
| | | 0.4-10 NM, BANDS 1-10 | W SWIDER RGP+SP V7 P573-94, 1969 | 60 |
| | | GAMMA- X-RAY PRE ELECT | SEE IONIZATION SECTION OF TEXT | 60 |
| | | 100-105 NM, BANDS 11-12 | ESTIMATED | 60 |
| | | 105-112 NM, BANDS 13-15 | R P WAYNE IN MMRE G FIOCCO ED P 240-52 1971 | 60 |

TABLE A9. BENCHMARK-76 PRODUCTION RATES FOR QUIESCENT CONDITIONS.
THE RATES ARE ZERO FOR REACTIONS 18-32, INCLUSIVE.

| REACTION NO. | 10 KM | 20 KM | 30 KM | 40 KM | 50 KM | 60 KM | 70 KM | 80 KM |
|---|---|---|---|---|---|---|---|---|
| 1 | 3.11E-02 | 3.13E-02 | 3.23E-02 | 3.36E-02 | 3.47E-02 | 3.49E-02 | 3.49E-02 | 3.50E-02 |
| 2 | 1.14E+00 | 1.15E+00 | 1.16E+00 | 1.17E+00 | 1.18E+00 | 1.18E+00 | 1.18E+00 | 1.18E+00 |
| 3 | 5.05E-02 | 5.21E-02 | 5.84E-02 | 6.70E-02 | 7.42E-02 | 7.57E-02 | 7.60E-02 | 7.60E-02 |
| 4 | 3.06E-01 | 3.08E-01 | 3.14E-01 | 3.20E-01 | 3.24E-01 | 3.25E-01 | 3.25E-01 | 3.25E-01 |
| 5 | 6.86E-02 | 6.89E-02 | 7.01E-02 | 7.14E-02 | 7.25E-02 | 7.28E-02 | 7.28E-02 | 7.28E-02 |
| 6 | 2.06E-01 | 2.07E-01 | 2.10E-01 | 2.12E-01 | 2.14E-01 | 2.14E-01 | 2.15E-01 | 2.15E-01 |
| 7 | 1.89E+00 | 1.90E+00 | 1.93E+00 | 1.94E+00 | 1.96E+00 | 1.96E+00 | 1.96E+00 | 1.96E+00 |
| 8 | 1.40E-02 | 1.41E-02 | 1.42E-02 | 1.43E-02 | 1.44E-02 | 1.44E-02 | 1.44E-02 | 1.44E-02 |
| 9 | 1.89E-01 | 1.90E-01 | 1.93E-01 | 1.94E-01 | 1.96E-01 | 1.96E-01 | 1.96E-01 | 1.96E-01 |
| 10 | 1.89E-01 | 1.90E-01 | 1.93E-01 | 1.94E-01 | 1.96E-01 | 1.96E-01 | 1.96E-01 | 1.96E-01 |
| 11 | 3.83E-04 | 4.16E-04 | 6.44E-04 | 1.14E-03 | 1.96E-03 | 2.16E-03 | 2.19E-03 | 2.20E-03 |
| 12 | 6.79E-02 | 6.82E-02 | 6.93E-02 | 7.06E-02 | 7.17E-02 | 7.20E-02 | 7.20E-02 | 7.20E-02 |
| 13 | 1.89E-01 | 1.90E-01 | 1.93E-01 | 1.94E-01 | 1.96E-01 | 1.96E-01 | 1.96E-01 | 1.96E-01 |
| 14 | 1.89E-01 | 1.90E-01 | 1.93E-01 | 1.94E-01 | 1.96E-01 | 1.96E-01 | 1.96E-01 | 1.96E-01 |
| 15 | 1.16E-01 | 1.17E-01 | 1.19E-01 | 1.20E-01 | 1.22E-01 | 1.22E-01 | 1.22E-01 | 1.22E-01 |
| 16 | 4.71E-01 | 4.74E-01 | 4.80E-01 | 4.87E-01 | 4.93E-01 | 4.94E-01 | 4.94E-01 | 4.95E-01 |
| 17 | 2.67E-01 | 2.69E-01 | 2.73E-01 | 2.76E-01 | 2.79E-01 | 2.79E-01 | 2.79E-01 | 2.79E-01 |
| ** | ******** | ******** | ******** | ******** | ******** | ******** | ******** | ******** |
| 33 | 0. | 0. | 0. | 0. | 0. | 2.65E-26 | 3.98E-15 | 2.72E-11 |
| 34 | 0. | 2.66E-20 | 3.25E-14 | 7.49E-12 | 8.19E-11 | 6.81E-10 | 1.31E-07 | 1.09E-06 |
| 35 | 3.09E-05 | 3.25E-05 | 4.42E-05 | 8.43E-05 | 1.49E-04 | 1.67E-04 | 1.72E-04 | 1.76E-04 |
| 36 | 5.87E-04 | 5.92E-04 | 6.03E-04 | 6.16E-04 | 6.27E-04 | 6.29E-04 | 6.29E-04 | 6.30E-04 |
| 37 | 6.83E-07 | 9.46E-07 | 9.13E-06 | 4.71E-05 | 9.66E-05 | 1.33E-04 | 1.67E-04 | 1.91E-04 |
| 38 | 1.87E-13 | 8.03E-08 | 3.21E-05 | 3.35E-04 | 8.48E-04 | 9.89E-04 | 1.03E-03 | 1.05E-03 |
| 39 | 0. | 0. | 7.48E-21 | 1.38E-13 | 2.55E-10 | 1.25E-08 | 1.25E-07 | 4.84E-07 |
| 40 | 1.02E-02 | 1.03E-02 | 1.05E-02 | 1.07E-02 | 1.08E-02 | 1.08E-02 | 1.08E-02 | 1.08E-02 |
| 41 | 0. | 0. | 0. | 0. | 0. | 0. | 0. | 0. |
| 42 | 3.23E-09 | 3.75E-09 | 4.01E-08 | 2.29E-07 | 4.61E-07 | 7.35E-07 | 1.22E-06 | 2.48E-06 |
| 43 | 4.38E-19 | 1.75E-13 | 7.30E-11 | 6.61E-10 | 1.31E-09 | 1.58E-09 | 3.18E-09 | 1.54E-08 |
| 44 | 0. | 0. | 0. | 0. | 2.35E-26 | 4.80E-14 | 2.05E-10 | 1.66E-09 |
| 45 | 0. | 0. | 0. | 0. | 0. | 0. | 0. | 0. |
| 46 | 0. | 0. | 0. | 0. | 0. | 0. | 0. | 0. |
| 47 | 3.27E-04 | 3.30E-04 | 3.34E-04 | 3.35E-04 | 3.35E-04 | 3.35E-04 | 3.35E-04 | 3.35E-04 |
| 48 | 6.67E-05 | 7.03E-05 | 7.60E-05 | 7.81E-05 | 7.84E-05 | 7.85E-05 | 7.85E-05 | 7.85E-05 |
| 49 | 7.06E-06 | 3.77E-05 | 4.28E-04 | 2.15E-03 | 8.09E-03 | 9.69E-03 | 9.90E-03 | 9.93E-03 |
| 50 | 1.80E-18 | 1.80E-18 | 1.80E-18 | 1.80E-18 | 1.90E-18 | 4.07E-18 | 1.93E-17 | 3.17E-16 |
| 51 | 3.87E-18 | 3.87E-18 | 3.87E-18 | 3.87E-18 | 4.07E-18 | 9.12E-12 | 3.89E-08 | 3.16E-07 |
| 52 | 5.94E-18 | 5.94E-18 | 5.94E-18 | 5.94E-18 | 6.25E-18 | 2.88E-13 | 1.23E-09 | 1.01E-08 |
| 53 | 6.84E-19 | 6.84E-19 | 6.84E-19 | 6.84E-19 | 7.20E-19 | 1.55E-18 | 7.33E-18 | 1.21E-16 |
| 54 | 0. | 0. | 0. | 0. | 0. | 0. | 0. | 0. |
| 55 | 2.92E-18 | 2.92E-18 | 2.92E-18 | 2.92E-18 | 3.07E-18 | 6.60E-18 | 3.13E-17 | 5.14E-16 |
| 56 | 2.07E-18 | 2.07E-18 | 2.07E-18 | 2.07E-18 | 2.18E-18 | 4.68E-18 | 2.22E-17 | 3.67E-16 |
| 57 | 2.94E-18 | 2.94E-18 | 2.94E-18 | 2.94E-18 | 3.09E-18 | 6.65E-18 | 3.15E-17 | 5.21E-16 |
| 58 | 1.20E-18 | 1.20E-18 | 1.20E-18 | 1.20E-18 | 1.26E-18 | 2.72E-18 | 1.29E-17 | 2.13E-16 |
| 59 | 0. | 0. | 0. | 0. | 0. | 0. | 0. | 0. |
| 60 | 2.94E-18 | 2.94E-18 | 2.94E-18 | 2.94E-18 | 3.09E-18 | 6.65E-18 | 1.20E-14 | 8.28E-11 |

DISTRIBUTION LIST

| No. of Copies | Organization |
|---|---|
| 12 | Commander<br>Defense Documentation Center<br>ATTN: DDC-TCA<br>Cameron Station<br>Alexandria, VA 22314 |
| 1 | Director<br>Institute for Defense Analyses<br>ATTN: Dr. E. Bauer<br>400 Army-Navy Drive<br>Arlington, VA 22202 |
| 2 | Director<br>Defense Advanced Research Projects Agency<br>ATTN: STO, CPT J. Justice,<br>Dr. S. Zakanyca<br>1400 Wilson Boulevard<br>Arlington, VA 22209 |
| 2 | Director of Defense Research and Engineering<br>ATTN: Mr. D. Brockway<br>CAPT K. Ruggles<br>Washington, DC 20305 |
| 4 | Director<br>Defense Nuclear Agency<br>ATTN: STAP (APTL)<br>STRA (RAAE)<br>Dr. C. Blank<br>Dr. H. Fitz, Jr.<br>DDST<br>Washington, DC 20305 |
| 2 | DASIAC/DOD Nuclear Information and Analysis Center<br>General Electric Company-TEMPO<br>ATTN: Mr. A. Feryok<br>Mr. W. Knapp<br>816 State Street<br>P.O. Drawer QQ<br>Santa Barbara, CA 93102 |
| 1 | Director<br>Defense Communications Agency<br>ATTN: Code 340, Mr. W. Dix<br>Washington, DC 20305 |
| 1 | Commander<br>US Army Materiel Development and Readiness Command<br>ATTN: DRCDMD-ST, N. Klein<br>5001 Eisenhower Avenue<br>Alexandria, VA 22333 |
| 1 | Commander<br>US Army Aviation Research and Development Command<br>ATTN: DRSAV-E<br>P.O. Box 209<br>St. Louis, MO 63166 |
| 1 | Director<br>US Army Air Mobility Research and Development Laboratory<br>Ames Research Center<br>Moffett Field, CA 94035 |
| 1 | Commander<br>US Army Electronics Research and Development Command<br>Technical Support Activity<br>ATTN: DELSD-L<br>Fort Monmouth, NJ 07703 |
| 1 | Commander<br>US Army Communications Rsch and Development Command<br>ATTN: DRDCO-SGS<br>Fort Monmouth, NJ 07703 |
| 3 | Commander/Director<br>US Army Electronics Research and Development Command<br>Atmospheric Sciences Laboratory<br>ATTN: Dr. D. E. Snider<br>Dr. F. E. Niles<br>Dr. M. G. Heaps<br>White Sands Missile Range, NM 88002 |

DISTRIBUTION LIST

| No. of Copies | Organization |
|---|---|
| 1 | Commander<br>US Army Missile Research and Development Command<br>ATTN: DRDMI-R<br>Redstone Arsenal, AL 35809 |
| 1 | Commander<br>US Army Missile Materiel Readiness Command<br>ATTN: DRSMI-AOM<br>Redstone Arsenal, AL 35809 |
| 1 | Commander<br>US Army Tank Automotive Research & Development Cmd<br>ATTN: DRDTA-UL<br>Warren, MI 48090 |
| 2 | Commander<br>US Army Armament Research and Development Command<br>ATTN: DRDAR-TSS (2 cys)<br>Dover, NJ 07801 |
| 1 | Commander<br>US Army Armament Materiel Readiness Command<br>ATTN: DRSAR-LEP-L, Tech Lib<br>Rock Island, IL 61299 |
| 1 | Commander, USACEEIA<br>ATTN: CCC-CED-EMED<br>Miles Merkel<br>Fort Huachuca, AZ 85635 |
| 2 | Commander<br>US Army Harry Diamond Labs<br>ATTN: DRXDO-TI<br>DRXDO-NP<br>Mr. F. Wimenitz<br>2800 Powder Mill Road<br>Adelphi, MD 20783 |
| 1 | Director<br>US Army TRADOC Systems Analysis Agency<br>ATTN: ATAA-SL, Tech Lib<br>White Sands Missile Range<br>NM 88002 |
| 3 | Commander<br>US Army Research Office<br>ATTN: Dr. A. Dodd, Dr. D. Squire<br>Dr. R. Lontz<br>P.O. Box 12211<br>Research Triangle Park, NC 27709 |
| 2 | Director<br>US Army BMD Advanced Technology Center<br>ATTN: Mr. M. Capps<br>Mr. W. Davies<br>P.O. Box 1500<br>Huntsville, AL 38507 |
| 2 | Commander<br>US Army BMD System Command<br>ATTN: SSC-HS, Mr. H. Porter<br>SSC-TET, Mr. E. Carr<br>P.O. Box 1500<br>Huntsville, AL 35807 |
| 1 | Director<br>US Army Ballistic Missile Defense Program Office<br>ATTN: Mr. C. McLain<br>5001 Eisenhower Avenue<br>Alexandria, VA 22333 |
| 1 | HQDA (DAEN-RDM/Dr. F. de Percin)<br>Washington, DC 20314 |
| 3 | Commanding Officer<br>US Army Research & Development Group (Europe)<br>ATTN: Dr. H. Lemons,<br>Dr. G. R. Husk,<br>LTC J. Kennedy<br>Box 15<br>FPO New York 09510 |

DISTRIBUTION LIST

| No. of Copies | Organization |
|---|---|
| 1 | Chief of Naval Research<br>ATTN: Code 418, Dr. J. Dardis<br>Department of the Navy<br>Washington, DC 20360 |
| 1 | Commander<br>US Naval Surface Weapons Center<br>ATTN: Dr. L. Rutland<br>Silver Spring, MD 20910 |
| 1 | Commander<br>US Naval Electronics Laboratory<br>ATTN: Mr. W. Moler<br>San Diego, CA 92152 |
| 4 | Commander<br>US Naval Research Laboratory<br>ATTN: Dr. W. Ali<br>Dr. D. Strobel<br>Code 7700, Mr. J. Brown<br>Code 2020, Tech Lib<br>Washington, DC 20375 |
| 4 | HQ USAF (AFNIN; AFRD; AFRDQ/ ARTAC/COL C. Anderson)<br>Washington, DC 20330 |
| 3 | AFGL (LKB, Dr. K. Champion, Dr. W. Swider, Dr. J. Paulson)<br>Hanscom AFB, MA 01730 |
| 2 | AFSC (DLCAW, LTC R. Linkous; SCS)<br>Andrews AFB, 20334 |
| 4 | Director<br>Los Alamos Scientific Laboratory<br>ATTN: Dr. W. Maier (Gp J-10)<br>Dr. J. Zinn (MS 664)<br>Dr. W. Myers<br>Dr. M. Peek<br>P.O. Box 1663<br>Los Alamos, NM 87544 |
| 2 | Sandia Laboratories<br>ATTN: Dr. K. J. Touryan<br>Dr. F. Hudson<br>P.O. Box 5800<br>Albuquerque, NM 87115 |
| 1 | Director<br>National Aeronautics and Space Administration<br>Goddard Space Flight Center<br>ATTN: Dr. R. Goldberg (Code 912)<br>Greenbelt, MD 20771 |
| 1 | Director<br>National Bureau of Standards<br>US Department of Commerce<br>ATTN: R. F. Hampson<br>Washington, DC 20234 |
| 2 | Director<br>National Science Foundation<br>ATTN: Dr. F. Eden<br>Dr. G. Adams<br>1800 G. Street, N.W.<br>Washington, DC 20550 |
| 1 | Calspan Corporation<br>ATTN: Mr. R. Fluegee<br>P.O. Box 235<br>Buffalo, NY 14221 |
| 2 | General Electric Company<br>Valley Forge Space Technology Center<br>ATTN: Dr. M. Bortner<br>Dr. T. Baurer<br>P.O. Box 8555<br>Philadelphia, PA 19101 |
| 1 | General Research Corporation<br>ATTN: Dr. J. Ise<br>P.O. Box 3587<br>Santa Barbara, CA 93105 |

DISTRIBUTION LIST

| No. of Copies | Organization |
|---|---|
| 2 | Lockheed Palo Alto Research Laboratory<br>ATTN: Dr. J. Reagan<br>Mr. R. Sears<br>3251 Hanover Street<br>Palo Alto, CA 94304 |
| 1 | Mission Research Corporation<br>ATTN: Dr. M. Scheibe<br>735 State Street<br>P.O. Drawer 719<br>Santa Barbara, CA 93102 |
| 1 | Mitre Corporation<br>ATTN: Tech Lib<br>P.O. Box 208<br>Bedford, MA 01730 |
| 1 | Pacific-Sierra Research Corp.<br>ATTN: Mr. E. Fields<br>1456 Cloverfield Blvd.<br>Santa Monica, CA 90404 |
| 1 | R&D Associates<br>ATTN: Dr. F. Gilmore<br>P.O. Box 9695<br>Marina Del Rey, CA 90291 |
| 1 | The Rand Corporation<br>ATTN: Dr. C. Crain<br>1700 Main Street<br>Santa Monica, CA 90406 |
| 2 | Science Applications, Inc.<br>ATTN: Mr. R. Lowen,<br>Mr. D. Hamlin<br>1250 Prospect Plaza<br>La Jolla, CA 90406 |
| 2 | Science Applications, Inc., Huntsville<br>ATTN: Mr. R. Byrn<br>Mr. D. Divis<br>2109 West Clinton Avenue<br>Huntsville, AL 358051 |
| 1 | Spectra Research Systems, Inc.<br>ATTN: Mr. B. Kilday<br>2212 Dupont Drive<br>Irvine, CA 92664 |
| 1 | Stanford Research Institute<br>ATTN: Dr. J. Peterson<br>333 Ravenswood Avenue<br>Menlo Park, CA 94025 |
| 1 | Systems Control, Inc.<br>ATTN: Mr. R. Foerster<br>260 Sheridan Avenue<br>Palo Alto, CA 94306 |
| 1 | Systems, Science & Software<br>ATTN: Dr. K.D. Pyatt, Jr.<br>P.O. Box 1620<br>La Jolla, CA 92037 |
| 1 | TRW Systems Group<br>ATTN: Tech Lib<br>One Space Park<br>Redondo Beach, CA 90278 |
| 1 | Visidyne, Inc.<br>ATTN: Dr. H. Smith<br>19 Third Avenue, N.W.<br>Industrial Park<br>Burlington, MA 01803 |
| 1 | University of Illinois<br>Department of Electrical Engineering<br>ATTN: Dr. C. Sechrist, Jr.<br>Urbana-Champaign Campus<br>Urbana, IL 61801 |
| 1 | University of Minnesota, Morris<br>Division of Science and Mathematics<br>ATTN: Dr. M. N. Hirsh<br>Morris, MN 56267 |
| 1 | University of Texas at El Paso<br>Physics Department<br>El Paso, TX 79902 |

DISTRIBUTION LIST

No. of Copies — Organization

1 Utah State University
Center for Research in Aeronomy
ATTN: Dr. L. Megill
Logan, UT 84321

1 Wayne State University
Department of Engineering
ATTN: Dr. R. Kummler
Detroit, MI 48202

Aberdeen Proving Ground

Dir, USAMSAA
Cdr, USATECOM
ATTN: DRSTE-SG-H